Title
EXPERIMENTS ON POLARIZATION IN SCATTERING DEUTERONS FROM COMPLEX NUCLEI AND IN PROTON-PROTON SCATTERING

Author
Baldwin, John A.

Publication Date
1956-05-11

UCRL 3412

UNIVERSITY OF CALIFORNIA

Radiation Laboratory

BERKELEY, CALIFORNIA

UCRL-3412

UNIVERSITY OF CALIFORNIA

Radiation Laboratory
Berkeley, California

Contract No. W-7405-eng-48

EXPERIMENTS ON POLARIZATION IN SCATTERING DEUTERONS FROM COMPLEX NUCLEI AND IN PROTON-PROTON SCATTERING

John A. Baldwin, Jr.

(Thesis)

May 11, 1956

Printed for the U. S. Atomic Energy Commission

Contents

EXPERIMENTS ON POLARIZATION IN SCATTERING DEUTERONS FROM COMPLEX NUCLEI AND IN PROTON-PROTON SCATTERING

John A. Baldwin, Jr.

Radiation Laboratory
University of California
Berkeley, California

May 11, 1956

ABSTRACT

The elastic double scattering of deuterons by complex nuclei has been investigated experimentally. Measurements were made on carbon, aluminum, and copper at around 157 Mev; on lithium, beryllium, and carbon at around 125 Mev; and on carbon and aluminum at 94 Mev. The expected tensor components of the deuteron polarization have not been observed. Measurements have been made of the differential cross section and vector-type polarization as a function of angle for the scattering of deuterons from the above elements, at the above energies. The observed polarizations were larger than would be expected on the basis of the individual nucleon-nucleus interactions.

In a second experiment we measured the 169-Mev proton-proton polarization at 10°, 15°, 22.5°, 30°, and 35° in the laboratory system. The results indicate that partial waves up to and including $L = 3$ are important at this energy.

INTRODUCTION

During the past several years the group of Chamberlain, Segrè, Wiegand and students has been studying experimentally neutron-proton and proton-proton scattering. The recent extraction of a polarized beam from the 184-inch cyclotron[1] has considerably increased the amount of information obtainable from such experiments. Indeed the information gained in the 310-Mev proton-proton double- and triple-scattering experiments[1,2,22] is sufficient to make determinate the equations for the phase shifts ($L \leqslant 3$, $J \leqslant 4$) in terms of experimentally determined quantities.[3,22]

It is interesting to extend these experiments to lower energies, since in this way one may learn something about the energy dependence of the proton-proton phase shifts. Chamberlain and Garrison[4,27] have investigated the angular distribution and Pettengill[5] has measured the total cross section at about 170 Mev. My experiment, designed to measure the proton-proton polarization at 169 Mev, is discussed in Sections I and III of this paper.

Considerable work has been done on proton-proton polarization by other laboratories and at different energies.[1,2,5,6,7,8,9,10,11,22]

The formalism and theory of the scattering of polarized protons by protons has been discussed by many authors. See, for example, References 12, 3, 21, 25.

In Sections I and II we deal with certain experiments which involve the elastic scattering of polarized deuterons from nuclei. Both in its experimental and in its theoretical features, this is more complicated than nucleon-nucleus double scattering. The second-scattered intensity of nucleons may be described by but one parameter in addition to the unpolarized cross section — namely the polarization. For deuterons, however — because they have spin 1 — four additional parameters may, in principle, be measured. The theoretical treatment of deuteron scattering must, of necessity, entail more approximations than that for protons because the deuteron is not an "elementary" particle. The problem is further complicated by the existence of both S and D states in the deuteron wave function.

In spite of the theoretical difficulties, the results of the deuteron experiments should lead to a better understanding of the nature of the spin-orbit interaction,[13] which is assumed to give rise to polarization phenomena, and of the energy dependence of the nucleon-nucleus interaction.[14]

The results of some earlier deuteron experiments at this laboratory have been reported in the Physical Review.[15] Lakin[16] has given a theoretical discussion of deuteron double scattering. Stapp,[3] using a formalism different from that of Lakin, has made an attempt to fit some of my data. He has considered contributions due to the first and second Born approximation as well as the presence of D state in the deuteron wave function.

Throughout this paper the symbol Θ is used to denote the (polar) scattering angle as measured in the laboratory system, and θ for that measured in the center-of-mass system. All other symbols used refer (unless otherwise indicated) to the laboratory system.

I. EXPERIMENTAL FEATURES COMMON TO BOTH DEUTERON AND PROTON EXPERIMENTS

A. Polarized Beam

The polarized beam is obtained by allowing the circulating beam to scatter from a target (Target 1) fastened to a probe inside the 184-inch cyclotron. The particles scattered outward are deflected in the fringing field of the cyclotron. Those particles scattered at a suitable angle pass through an aperture in the vacuum tank into an evacuated tube where they encounter, in order, the following: a set of collimating blocks (premagnet collimator), a bending (or steering) magnet, a lens consisting of strong-focusing quadrupole magnets, a 46-inch-long tubular collimator (snout collimator), and finally a thin Al foil vacuum window. The particles pass through this foil into the experimental area (cave) where the second scattering is done. The first scattering of deuterons was done from the main probe of the cyclotron (Position a, Fig. 1). The first scattering for protons was done at a position two feet upstream from the main probe position (Position b, Fig. 1), from a beryllium target. This second position (b) was used for protons since it yielded a more highly polarized beam of equal intensity.

Calculations performed by Dr. T. J. Ypsilantis indicated that particles elastically scattered at an angle of 17^{o} from the main probe position (a) and 13^{o} from the second position (b) would reach the exit tube.[22] After the cyclotron had been shut down for conversion, however, I used a mechanical analogue orbit plotter and found angles of 16 ± 0.5^{o} and 10.25 ± 0.25^{o} respectively for the first-scattering angles; the widths were determined by the width of the exit tube at its entrance to the vacuum tank. For the main probe position, the error in the first scattering angle corresponding to a radial error in probe position of 0.5 in. was determined to be $\sim 1^{o}$.

B. Energy Degradation

To obtain the 174-Mev proton beam and the 133- and 100-Mev deuteron beams, it was necessary to degrade the full-energy beam. In all cases but one (explained in Section III-D) the degradation was done inside the vacuum tank by placing beryllium bricks on a movable cart in such a position as to intercept the first scattered beam (Position A in Fig. 1). Beryllium was used to minimize intensity loss due to multiple scattering.

One is led to inquire into the effect of degradation on the beam polarization. Calculations by Wolfenstein[24] indicate that this effect is small. One might also wonder if, owing to the changed magnetic rigidity of the particles after passing through the degrader, the exit tube might accept particles whose first scattering angle is different from the assumed one. Calculations indicate that this effect is also small. An experimental check (described in Section III-D) was performed and seemed to confirm the expectation that the polarization of the degraded beam is substantially the same as that of the full-energy beam.

Degradation at Position A is preferred over that at Position B, since—owing to the magnetic selection in the steering magnet—the resulting beam has a smaller energy spread and has less neutron contamination than the beam degraded at Position B.

The beam energy was determined from a Bragg curve[31] taken with two argon-filled ion chambers.

C. Apparatus

Figure 2 shows schematically the positioning of the equipment used in the second scattering. The beam was usually monitored with an ion chamber.[31] However, for measurements at small angles ($\leqslant 4^{\circ}$), two large counters in coincidence were placed in the beam for this purpose. These are referred to as Counters A and B. To measure the scattered intensity a 3-counter telescope was used. These counters were called Counters 1, 2 and 3; Number 1 was defining and was closest to the target. A variable copper absorber was put between Counters 1

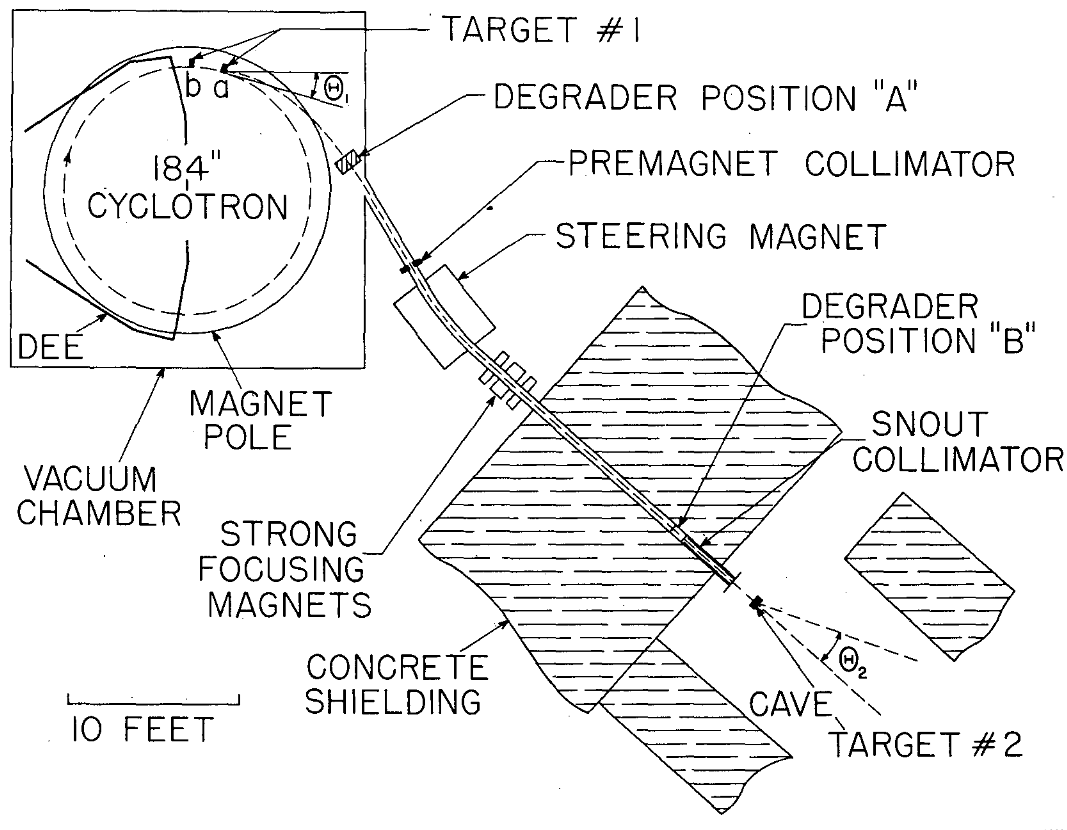

Fig. 1. Celebrated figure showing plan view of cyclotron and path of polarized beam.

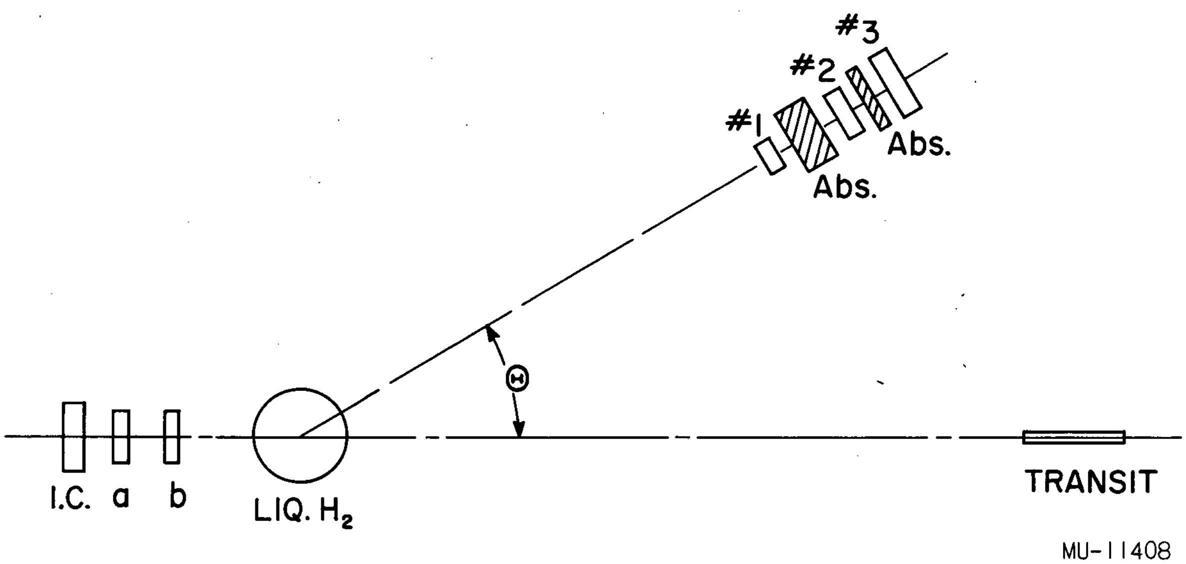

Fig. 2. Disposition of target and counters in second scattering.

and 2. A small fixed absorber was sometimes inserted between Counters 2 and 3. Each counter consisted of a slab of plastic scintillator viewed by 1P21 photomultiplier tubes. Counters A and B used one tube each. Counters 1, 2 and 3 used two tubes each, one on each end. The scintillator dimensions were:

A and B 3 by 3 by 1/4 in.,

1 6 by 1 by 1/4 in.,

2 8 by 2.5 by 3/8 in.,

3 9 by 3 by 3/8 in.

The signal from each counter was sent to the counting area, where it was passed through a variable-delay box and amplified by a pair of Hewlett-Packard Model 460A amplifiers. The amplified signals were fed into a coincidence circuit designed and built by Dr. Clyde Wiegand. The coincidence circuit is capable of making simultaneously A-B, 1-2-3, and 1-2 coincidences. The coincidence outputs were fed through linear amplifiers into scalers.

The charge liberated in the ion chamber was collected on a calibrated capacitor. The voltage across the capacitor was measured by a dc feedback electrometer and recorded on a self-calibrating Speedomax recorder.

D. Counting Procedure

Both the 1-2 and 1-2-3 coincidence counting rates were recorded. The telescope absorber was usually chosen so as to make the 1-2-3 rate meaningful. The 1-2 rate was as a check on the workings of the electronics and as an indication of the effect of inelastic scattering.

For each polar angle Θ and azimuthal angle ϕ, three counting rates were usually measured. These were:

"Target." The counting rate observed with the target in place.

"Blank." The counting rate observed with a blank target in place. In the proton-proton experiment this blank target was similar to the hydrogen target except that it contained no hydrogen. In scattering from nuclei, the blank target consisted of no target at all. In either case, however, an absorber equal in stopping power to the target was added to the telescope absorber, since it was felt that most of the background originated from particles that had traversed the target.

"Accidentals." The counting rate observed with the target in place but with an extra delay equal to the cyclotron rf pulse repetition time introduced into the circuit of counter No. 1. Counter No. 1 was used because, since it is unprotected by absorbers, its beam-derived counting rate is higher than that in the other two counters. The accidental rate was generally negligible in scattering from nuclei. The delay used was 6×10^{-8} sec for the proton beam and 10×10^{-8} sec for the deuteron beam.

The counting rate due to the target, $\mathcal{J}(\Theta, \phi)$, was then taken to be $\mathcal{J}$ = (Target) - (Blank) - (Accidental).

The counting rates were used to derive three quantities. These were:

(a) The asymmetry, or coefficient of $\cos \phi$ in the angular distribution; denoted by e:

$$e(\Theta) = \frac{\mathcal{J}(\Theta, 0^{\circ}) - \mathcal{J}(\Theta, 180^{\circ})}{\mathcal{J}(\Theta, 0^{\circ}) + \mathcal{J}(\Theta, 180^{\circ})}$$

(b) The coefficient of $\cos 2\phi$, denoted by B:

$$B(\Theta) = \frac{[\mathcal{J}(\Theta, 0^{\circ}) + \mathcal{J}(\Theta, 180^{\circ})] - [\mathcal{J}(\Theta, 90^{\circ}) + \mathcal{J}(\Theta, 270^{\circ})]}{[\mathcal{J}(\Theta, 0^{\circ}) + \mathcal{J}(\Theta, 180^{\circ})] + [\mathcal{J}(\Theta, 90^{\circ}) + \mathcal{J}(\Theta, 270^{\circ})]}$$

(c) The average counting rate, denoted by $\bar{\mathcal{J}}$:

$$\bar{\mathcal{J}}(\Theta) = \frac{1}{4}[\mathcal{J}(\Theta, 0^{\circ}) + \mathcal{J}(\Theta, 90^{\circ}) + \mathcal{J}(\Theta, 180^{\circ}) + \mathcal{J}(\Theta, 270^{\circ})],$$

or

$$\bar{\mathcal{J}}(\Theta) = \frac{1}{2}[\mathcal{J}(\Theta, 0^{\circ}) + \mathcal{J}(\Theta, 180^{\circ})].$$

Since the first scattering is to the left (as seen by the particles, standing upright), $\phi = 0^{\circ}$ is defined as scattering to the left, $\phi = 90^{\circ}$ is scattering up, etc. The second-scattered intensity is assumed to have the following dependence:

for deuterons, $\mathcal{J}(\Theta, \phi) = \mathcal{J}_0(\Theta)\,[\,1 + \alpha + e \cos\phi + B \cos 2\phi\,]$;

for protons, $\mathcal{J}(\Theta, \phi) = \mathcal{J}_0(\Theta)\,[\,1 + e \cos\phi\,]$;

where $\mathcal{J}_0$ is the scattered intensity observed with an unpolarized beam.

In general, the symbol $\mathcal{J}$ denotes a scattered intensity, and the symbol I a differential scattering cross section. Where the distinction is unimportant, we use the symbol I indiscriminately.

II. DEUTERON-NUCLEUS DOUBLE SCATTERING

A. Theoretical

1. Formalism

Since the polarization formalism for particles of spin 1 is much less commonplace than that for particles of spin 1/2, it seems worth while to spend a little time discussing some aspects of it.

The familiar scattered amplitude $f(\theta, \phi)$ of Schiff[17] may be expressed in component form in various ways. For example, one may consider components labeled by orbital angular momentum, total angular momentum, spin, parity, etc. In many cases it is useful to deal with components of $f(\theta, \phi)$ in the spin space of the system. Lakin[16] considers such a decomposition for the problem in which a spin-1 particle is elastically scattered from a target nucleus of arbitrary spin. Following his treatment, we shall briefly discuss the scattering of deuterons from a target of spin zero. The treatment for the general case of arbitrary target spin differs little from our special case. The final results are, moreover, the same, inasmuch as the spin of the target nucleus is generally neglected in writing the Hamiltonian for the interaction of nucleons with nuclei.

Let us now consider our wave functions as spinors, having components labeled by the magnetic quantum number m for a particle of spin 1. It is a general postulate of quantum mechanics that the final state of a system evolves linearly from its initial state. We therefore represent the final wave function as the result of a linear operation on the initial wave function. This linear operation must be a matrix in the spin space of the deuteron. We call this operator the scattering matrix and denote it by M. If the incident wave function is

$$\psi_i = e^{ikz} \chi ,$$

where χ is a 3-component column spinor representing the spin part of the wave function of the deuteron beam, then the final wave is

$$\psi_f \underset{r \to \infty}{\simeq} e^{ikz} \chi + \frac{1}{r} e^{ikr} M \chi .$$

It is obvious that there are nine linearly independent 3-by-3 matrices. We wish to find a convenient set of linearly independent 3-by-3 matrices in order to be able to express our operators as linear combinations of them. A set from which to start is: $1, S_x, S_y, S_z$ where 1 is the 3-by-3 unit matrix and the S_i are the Cartesian components of the spin-1 angular-momentum operator in matrix representation. The remaining operators may be formed by defining the six operators:[3, 18]

$$S_{ij} = \frac{1}{2}(S_i S_j + S_j S_i) - (2/3)\, 1\, \delta_{ij}$$

This, however, gives us a total of ten operators, among which there must exist a linear relation. Various subterfuges may be employed to circumvent this difficulty. A more convenient set is formed by Lakin in the following way: The basic matrices are called T_{JM} and are formed from $1, S_x, S_y$ and S_z in a way that is analogous to the formation of the spherical harmonics from 1, x, y, and z. Thus,

$$T_{00} = 1 = \begin{pmatrix} 1 & 0 & 0 \\ 0 & 1 & 0 \\ 0 & 0 & 1 \end{pmatrix},$$

$$T_{11} = -\frac{\sqrt{3}}{2}(S_x + iS_y) = -\sqrt{\frac{3}{2}}\begin{pmatrix} 0 & 1 & 0 \\ 0 & 0 & 1 \\ 0 & 0 & 0 \end{pmatrix},$$

$$T_{10} = \sqrt{\frac{3}{2}}\, S_z = \sqrt{\frac{3}{2}}\begin{pmatrix} 1 & 0 & 0 \\ 0 & 0 & 0 \\ 0 & 0 & -1 \end{pmatrix},$$

$$T_{22} = \frac{\sqrt{3}}{2}(S_x + iS_y)^2 = \sqrt{3}\begin{pmatrix} 0 & 0 & 1 \\ 0 & 0 & 0 \\ 0 & 0 & 0 \end{pmatrix},$$

$$T_{21} = -\frac{\sqrt{3}}{2}[(S_x + iS_y)S_z + S_z(S_x + iS_y)] = -\sqrt{\frac{3}{2}}\begin{pmatrix} 0 & 1 & 0 \\ 0 & 0 & -1 \\ 0 & 0 & 0 \end{pmatrix},$$

$$T_{20} = \frac{1}{\sqrt{2}}(3S_z^2 - 2) = \frac{1}{\sqrt{2}}\begin{pmatrix} 1 & 0 & 0 \\ 0 & -2 & 0 \\ 0 & 0 & 1 \end{pmatrix},$$

$$T_{J,-M} = (-1)^M\, T^{\dagger}_{J,M} .$$

It is to be noted that J and M are simply parameters that number the matrices and have nothing to do with the angular momentum of the system.

Let us denote by $\langle T_{JM} \rangle$ the quantum mechanical expectation value of T_{JM} averaged over the particles of a beam. Since the T_{JM} constitute a complete set of spin operators, the specification of the $\langle T_{JM} \rangle$ for a beam of deuterons completely describes the polarization state of the beam.

For a beam of unpolarized deuterons, all the $\langle T_{JM} \rangle$ are zero except $\langle T_{00} \rangle$, the unit operator. If we scatter a beam of unpolarized deuterons and examine the portion of the scattered flux in the neighborhood of some mean scattering angle, we may expect this "beam" to be characterized by some nonzero $\langle T_{JM} \rangle$, which are, of course, functions of the scattering angle.

Consider the following double-scattering experiment. A beam of unpolarized deuterons is incident upon target No. 1, with an initial propagation vector $\vec{k}_{1i}$ (where the momentum of a particle is $\vec{p} = \hbar \vec{k}$). Let that portion of the scattered flux near some final propagation vector, $\vec{k}_{1f}$, be incident upon a target No. 2. Let us measure the second scattered flux near some final propagation vector, $\vec{k}_{2f}$ (the initial second-scattering propagation vector, $\vec{k}_{2i} = \vec{k}_{1f}$, neglecting energy loss in the targets). If one sets up, for the second scattering, a right-handed coordinate system whose z axis is along $\vec{k}_{2i}$ and whose y axis is along the normal to the first scattering plane, $\vec{n}_1 = \vec{k}_{1i} \times \vec{k}_{1f}$, then—as Lakin shows—the second-scattered intensity is given by*

$$I = I_0 \,[1 + \langle T_{20} \rangle_1 \langle T_{20} \rangle_2 + 2 \,(- \langle T_{21} \rangle_1 \langle T_{21} \rangle_2 + i\langle T_{11} \rangle_1 \, i\langle T_{11} \rangle_2) \cos \phi, + 2 \langle T_{22} \rangle_1 \langle T_{22} \rangle_2 \cos 2\phi \,] .$$

The index on $\langle T_{JM} \rangle$ indicates that the parameter is characteristic of either the first or second scattering; ϕ is the angle between the normals to the two scattering planes: $\vec{n}_1 \cdot \vec{n}_2 = n_1 n_2 \cos \phi$. I_0 is the unpolarized differential scattering cross section for the second scattering.

It is shown that if the first scattering does produce any nonzero $\langle \vec{S} \rangle$, it is directed along the y-axis. As a result $\langle T_{11} \rangle$ is pure

---

* Notice that the sign of the $\langle T_{21} \rangle$ term is given incorrectly in Lakin's paper.

imaginary: $\langle T_{11}\rangle = -\, i/2\sqrt{3}\, \langle S_y\rangle$. The $\langle T_{2M}\rangle$ are all real.

$i\,\langle T_{11}\rangle$ is referred to as vector polarization, since it is the expectation value of the y-component of the vector $\vec{S}$. The $\langle T_{2M}\rangle$ are referred to as components of the tensor polarization, since the T_{2M} are compounded from the elements of the second-rank tensor S_iS_j.

2. Impulse Approximation

Let us attempt to apply the impulse approximation[19, 20, 32] to a model similar to that used by Fermi[13] in connection with scattering of nucleons.

We assume charge independence. Then the interaction of a proton with a nucleus is identical with that of a neutron. We also assume that the Hamiltonian may be written

$$H = T_1 + T_2 + U_d(r_{12}) + V(\vec{r}_1, \vec{p}_1, \vec{\sigma}_1) + V(\vec{r}_2, \vec{p}_2, \vec{\sigma}_2),$$

where 1 and 2 label the neutron and proton of the deuteron,

T is the kinetic energy operator,

$r_{12} = \left|\vec{r}_1 - \vec{r}_2\right|$ = separation of the nucleons of the deuteron,

$U_d(r_{12})$ is the interaction between the nucleons of the deuteron,

and V is the interaction of a nucleon with the target nucleus.

We then write

$$\begin{aligned} H &= H_0 + H_1, \\ H_0 &= T_1 + T_2 + U_d(r_{12}), \\ H_1 &= V(1) + V(2). \end{aligned}$$

The initial and final wave functions may be written

$$\psi_i = \exp\left[i\vec{k}_i \cdot \tfrac{1}{2}(\vec{r}_1 + \vec{r}_2)\right] F(r_{12})\, \chi_1^{m_i}$$

$$\psi_f = \exp\left[i\vec{k}_f \cdot \tfrac{1}{2}(\vec{r}_1 + \vec{r}_2)\right] F(r_{12})\, \chi_1^{m_f},$$

where $F(r_{12})$ is the deuteron wave function (assumed to be pure S-state), and χ_1^{m} is the spinor representing unit angular momentum, with magnetic quantum number m. In the Born approximation, the scattering matrix is given as the matrix element of H_1 connecting the initial and final eigenstates of H_0:

$$M = -\frac{2M_d}{4\pi\hbar^2}\int d\vec{r}_1\, d\vec{r}_2\, F^*\exp\left[-i\vec{k}_f \cdot \tfrac{1}{2}(\vec{r}_1 + \vec{r}_2)\right][V(1) + V(2)]$$
$$\exp\left[i\vec{k}_i \cdot \tfrac{1}{2}(\vec{r}_1 + \vec{r}_2)\right] F,$$

where M_d is the deuteron reduced mass. Let us write V as a central potential plus a spin-orbit term:

$$V = U(r) + \vec{\sigma} \cdot [-\nabla Y(r)] \times \vec{p} \, \frac{\lambda_c^2}{\hbar} ,$$

where λ_c is $\frac{1}{2\pi}$ times the nucleon Compton wave length, and is introduced so that Y has the dimensions of energy. We then obtain for the scattering matrix the expression

$$M = f^{1/2}(K) \left[2g_d(K) + h_d(K,k) \vec{S} \cdot \vec{n} \right] .$$

The momentum transfer of the whole deuteron in the c.m. system is $\hbar K$; $K = \left| \vec{k}_f - \vec{k}_i \right| = 2k \sin \frac{1}{2}\theta$; f (K) is the sticking factor.[20] In the Born approximation g_d and h_d are given by

$$g_d(K) = - \frac{2M_d}{4\pi\hbar^2} \int d\vec{r} \, e^{-i\vec{K} \cdot \vec{r}} U(r) ,$$

$$h_d(K,k) = i\lambda_c^2 \, k^2 \sin\theta \left[- \frac{2M_d}{4\pi\hbar^2} \right] \int d\vec{r} \, e^{-i\vec{K} \cdot \vec{r}} Y(r) .$$

The scattering matrix describing the scattering of free nucleons by the potential V is

$$M = g_n(K) + h_n(K,k) \vec{\sigma} \cdot \vec{n} .$$

In the Born approximation g_n and h_n are given by

$$g_n(K) = - \frac{2M_n}{4\pi\hbar^2} \int d\vec{r} \, e^{-i\vec{K} \cdot \vec{r}} U(r) ,$$

$$h_n(K,k) = i\lambda_c^2 \, k^2 \sin\theta \left[- \frac{2M_n}{4\pi\hbar^2} \right] \int d\vec{r} \, e^{-i\vec{K} \cdot \vec{r}} Y(r) .$$

Thus we may express the elements of the deuteron scattering matrix in terms of the elements of the nucleon scattering matrix at the same momentum transfer:

$$g_d(K) = \frac{M_d}{M_n} g_n(K) ,$$

$$h_d(K, k_d) = \left(\frac{k_d}{k_n}\right)^2 \frac{\sin \theta_d}{\sin \theta_n} \frac{M_d}{M_n} h_n(K, k_n) .$$

Later we will compare the predictions of the above approximation with our experimental results. We will estimate $g_n(K)$ and $h_n(K, k_n)$, using the results of proton-nucleus scattering experiments. In the scattering of deuterons of momentum k_d, the nucleons that compose the deuteron interact with the target nucleus at an average momentum $k_n = \frac{1}{2} k_d$. (This is smeared out because of the internal momentum of the deuteron.) In making our comparison, then, we must use proton experiments at an energy about half that of the associated deuteron results.

We must now relate the $\langle T_{JM} \rangle$ resulting from the scattering of an unpolarized beam of deuterons to our g_d and h_d. Lakin shows that

$$MM^\dagger = \sum_{JM} \langle T_{JM} \rangle T_{JM}^\dagger .$$

We therefore expand $MM^\dagger$ in terms of $T_{JM}^\dagger$ and equate the coefficients in the expansion to the associated $\langle T_{JM} \rangle$:

$$MM^\dagger = f \left[4 \left| g_d \right|^2 + 2 (g_d^* h_d + g_d h_d^*) S_y + \left| h_d \right|^2 S_y^{\,2} \right].$$

Using the relations

$$S_y = - \frac{i}{\sqrt{3}} [T_{11}^\dagger + T_{1-1}^\dagger] ,$$

$$S_y^2 = - \frac{1}{2\sqrt{3}} [T_{22}^\dagger + T_{2-2}^\dagger] + \frac{2}{3} - \frac{1}{3\sqrt{2}} T_{20}^\dagger ,$$

We determine

$$I_0 = f\ [\,4\,|g_d|^2 + \frac{2}{3}\,|h_d|^2\,],$$

$$I_0\ i\langle T_{11}\rangle = \frac{2}{\sqrt{3}}\ f\ (g_d^* h_d + g_d h_d^*)\ ,$$

$$I_0\ \langle T_{22}\rangle = -\frac{1}{2\sqrt{3}}\ f\,|h_d|^2\ ,$$

$$I_0\ \langle T_{20}\rangle = -\frac{1}{3\sqrt{2}}\ f\,|h_d|^2\ ,$$

$$I_0\ \langle T_{21}\rangle = 0.$$

We have expressed the parameters characterizing deuteron-nucleus double scattering in terms of the proton-nucleus scattering matrix at the same center-of-mass momentum transfer, K. We refer to this subject again in Section II-I.

B. Apparatus

In all the deuteron runs a snout collimator of circular cross section was used, in order to obtain a beam with high azimuthal symmetry. A 1-inch-diameter collimator was used when possible, in order to obtain good angular and energy resolution. On the low-energy experiments, however, a collimator of 2-inch diameter was required for sufficient beam intensity.

The scattering table is so constructed as to be capable of rotation about an axis which can be brought into coincidence with the axis of the beam. This axis is marked by front and rear cross hairs. Figure 3 shows the scattering table.

C. Alignment

After the scattering table was approximately aligned by eye, x-ray films were exposed to the beam at the positions of the front and rear cross hairs. The centers of the beam spots were determined and marked. A transit placed in the rear of the cave was lined up on these

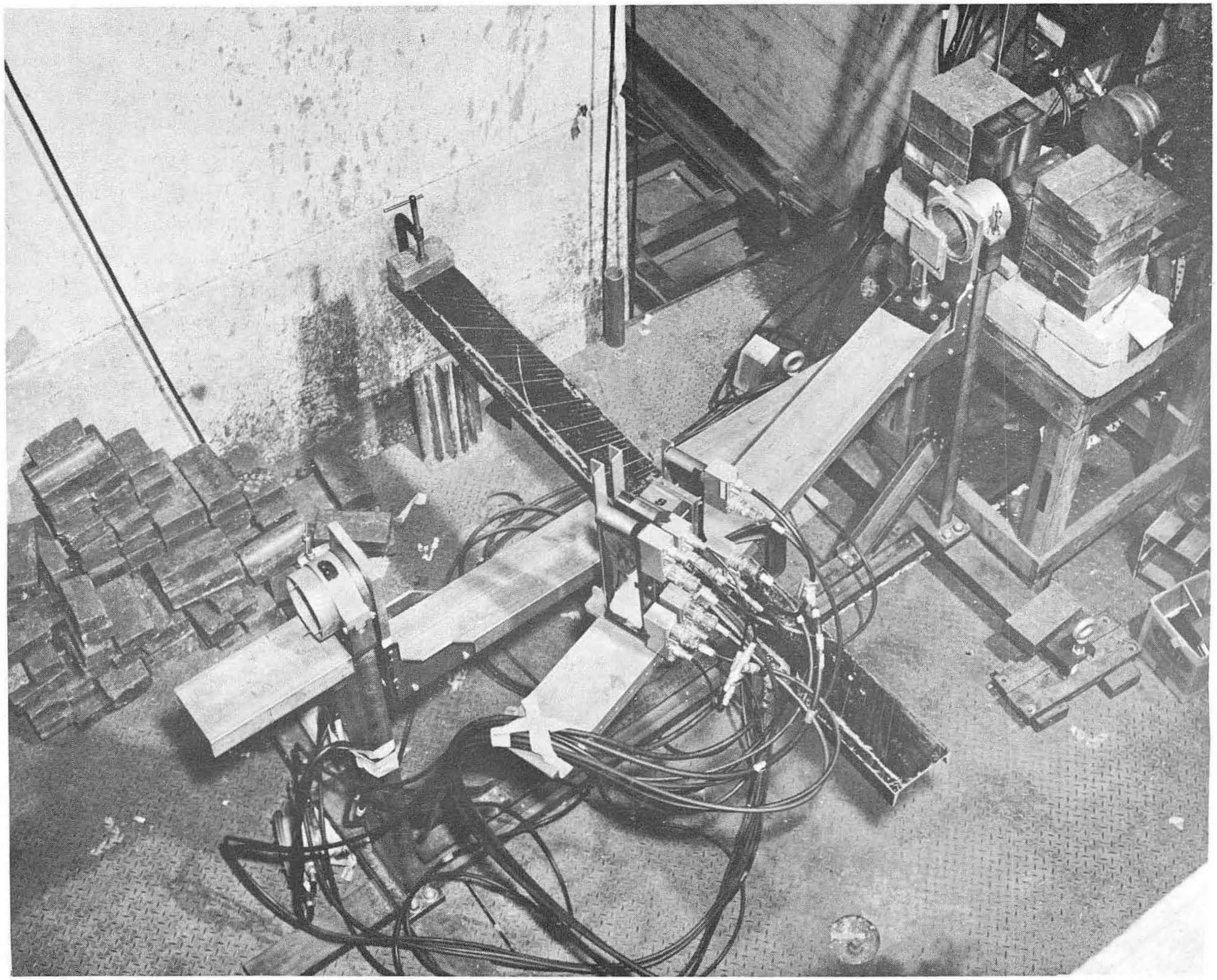

ZN-1257

Fig. 3. Scattering table and counter telescope used in deuteron experiment.

two points. With the transit defining the beam axis, the table was moved to bring the cross hairs into coincidence with the beam axis. Then, with counters A and B used as a monitor, the counting rate was measured for small angles for a number of values of Θ , and for $\phi = 0^{\circ}$, 90°, 180°, and 270°. In the multiple scattering region, the counting rate is a very sensitive function of Θ. Figure 4 shows typical results of such a measurement. Small adjustments were then made in the position of the rear of the table to equalize the 0°, 90°, 180°,and 270° counting rates.

D. Range Curve

A plot of counting rate vs. telescope absorber is called a range curve. Figure 5 shows a deuteron range curve. The counting rate initially decreases slowly owing to nuclear attenuation in the absorber. Later it decreases more rapidly owing to range stopping. These two portions can generally be approximated by straight lines. The intersection of these lines is called the "knee". The absorber value at which the counting rate drops to half its value at the knee is called the "mean range" in the telescope. The absorber value at which the second straight line reaches zero is called the "extrapolated range". The difference between the extrapolated and mean ranges gives a measure of the energy spread of the beam.

For each run a range curve was taken in the beam, with the A and B counters used as a monitor. Two pieces of information were extracted from the range curve. The first was the number by which the observed counting rate should be multiplied in order to obtain the counting rate extrapolated to zero absorber. This is needed to compute cross sections. Secondly, the range curve is used to determine a safe absorber value at which to run. In order to insure that one is counting elastic, or nearly elastic, scattering, he would like to operate at a point beyond the knee. There are two objections to this. First, beyond the knee, the counting rate is a sensitive function of beam energy. Small fluctuations in energy would lead to large systematic errors. The second objection centers around the existence of an energy gradient

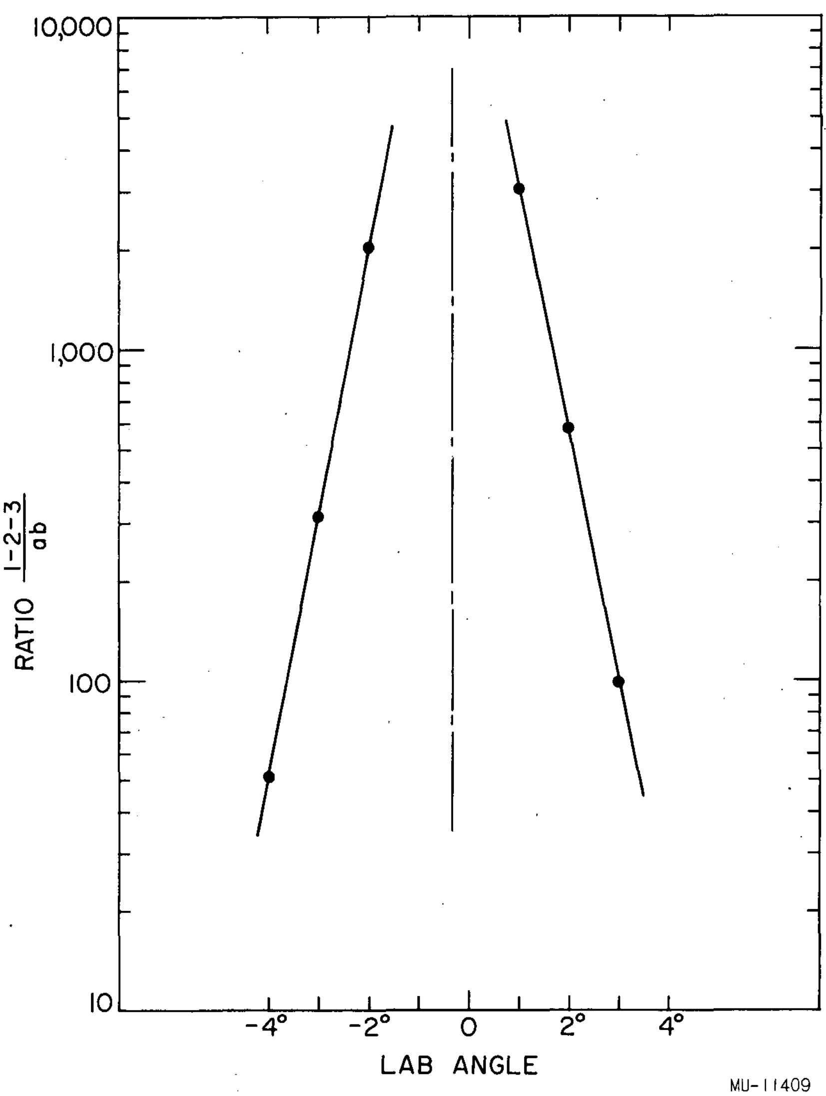

Fig. 4. Typical results of small-angle counting-rate measurement.

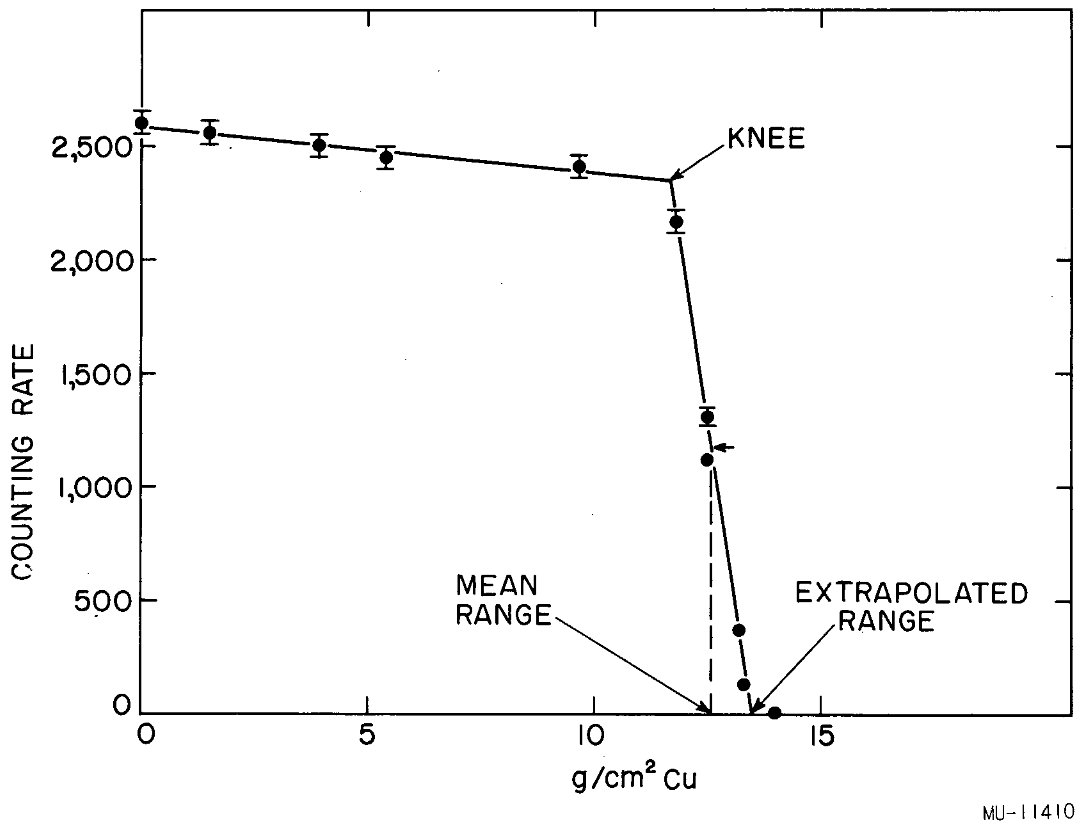

Fig. 5. Typical deuteron range curve.

of about 1.5 Mev/in. across the beam profile, due to the momentum sorting in the steering magnet. When one operates beyond the knee, he discriminates against the low-energy side of the beam. He thus makes the position of the beam center depend upon beam energy, telescope absorber, and target thickness. In practice, I compromised by operating as close to the knee as I felt I could and not discriminate energywise against any beam particles. In changing Θ, I corrected the absorber for recoil and target thickness changes.

E. Angular Resolution

The geometrical angular resolution was computed by folding together the effect of a circular aperture the size of the snout collimator and that of a rectangular aperture the size of the defining counter. The effect of multiple Coulomb scattering was taken from Millburn and Schecter.[30] The total was obtained by taking the square root of the sum of the squares of the two rms angles. The results agree reasonably well with the values obtained experimentally by sweeping the counters through the beam.

F. Beam Polarization

In the Appendix we discuss the effect of the magnetic fields encountered by the polarized beam on the beam polarization. We find that there is no effect on the vector polarization, $i\langle T_{11}\rangle$. The fields do, however, effect a mixing of the $\langle T_{2M}\rangle$. This effect is so small that we may neglect it.

The only nonzero $\langle T_{JM}\rangle$ uncovered by these experiments are related to the asymmetry e by the expression

$$e = 2\,[\,-\langle T_{21}\rangle_1 \langle T_{21}\rangle_2 + i\langle T_{11}\rangle_1\, i\langle T_{11}\rangle_2\,] .$$

If one performed an experiment in which he deflected the polarized beam by a large angle by means of a magnetic field, he could determine how much of e was produced by $\langle T_{21}\rangle$ and how much by $i\langle T_{11}\rangle$.

As no such experiment was done, because of the large deflections required, it is impossible to disentangle, in the asymmetry, the parameters characterizing the first and second scatterings. We would like to go farther than simply listing the observed asymmetries. To this end, we make a heuristic assumption. We assume $|\langle T_{21}\rangle| << 1$ at the angle of the first scattering. This allows us to say $\langle T_{21}\rangle_1 \langle T_{21}\rangle_2 \simeq 0$. There are the following reasons to think that this is so:

1. The first Born approximation predicts $\langle T_{21}\rangle \equiv 0$;

2. The experiment reported here shows that the other $\langle T_{2M}\rangle$ are small;

3. The calculations by Stapp[3] indicate that $\langle T_{21}\rangle$ should be small compared with $i\langle T_{11}\rangle$.

The asymmetry is now given by

$$e = 2\, i\langle T_{11}\rangle_1 \; i\langle T_{11}\rangle_2 \doteq 3/2 \langle S_y\rangle_1 \langle S_y\rangle_2 ,$$

since $T_{11} = -1/2\sqrt{3}\,(S_x + iS_y)$ and in our coordinate system $\langle S_x\rangle = 0$. We now have a relation which looks very similar to that holding for spin-1/2 particles, in which e depends on the product of a number that is characteristic of the beam and another that is characteristic of the target. In the spirit of this approximation, we may speak of a beam polarization (referring to the value of $i\langle T_{11}\rangle$ characterizing the beam) and list values of $i\langle T_{11}\rangle$ for various targets, energies, etc.

When Group I* experiments were done Θ_1 was believed to be 18^o. The remaining runs assumed 17^o. It was not till too late that the value 16^o was discovered. As a consequence, although a great deal of attention was paid to $\Theta_2 = 18^o$ and 17^o, little was paid to 16^o. There was, in fact, only one instance of double scattering at this angle in which the two scatterings were identical. This was at 156 Mev, Al-Al (Group I). The polarizations of all other beams were derived from this. The beam polarizations arrived at in this way are in fairly good agreement with those obtained by interpolation. The beam polarization statistics have been included in the error assigned to the tabulated values of $i\langle T_{11}\rangle$. These are consequently larger than they should have been.

---

* The Group designations are explained in Section II-I and Table VI.

One other point should be noted. The polarized proton beam is usually obtained by scattering at $\sim 10^{\circ}$ from beryllium. The polarization changes about 4.5% per degree in this region. In the deuteron experiments, the first target most commonly used was carbon. At the first-scattering angle 16°, $i\langle T_{11}\rangle$ is changing about 15.5% per degree. This makes the deuteron results more strongly dependent upon errors in probe position, cyclotron main field, etc.

G. Procedures

The second-scattered angular distribution has been expressed in terms of the previously defined experimental parameters α, B, e, and I_0 as

$$I = I_0 \left[1 + \alpha + e \cos\phi + B \cos 2\phi \right],$$

and in terms of theoretical parameters as

$$I = I_0 \left[1 + \langle T_{20}\rangle_1 \langle T_{20}\rangle_2 + 2\left(-\langle T_{21}\rangle_1 \langle T_{21}\rangle_2 + i\langle T_{11}\rangle_1 \; i\langle T_{11}\rangle_2 \right) \cos\phi + 2\langle T_{22}\rangle_1 \langle T_{22}\rangle_2 \cos 2\phi \right].$$

The first experiments were designed to measure e and B. To do this one simply measured the counting rates at $\phi = 0^{\circ}$, 90°, 180°, and 270°. As it became more apparent that B was very small, attention was concentrated on $\phi = 0^{\circ}$ and 180°.

The measurement of α required two separate experiments, one with a polarized beam and one with an unpolarized beam. For a polarized beam,

$$\bar{I}_p = 1/4 \left[I(0^{\circ}) + I(90^{\circ}) + I(180^{\circ}) + I(270^{\circ}) \right] = I_0 (1 + \alpha),$$

and for an unpolarized beam,

$$\bar{I}_u = I_0 .$$

Thus we have

$$\alpha = \frac{\bar{I}_p}{\bar{I}_u} - 1.$$

In order to make the two experiments as similar as possible, special precautions were taken. The same target and telescope absorber were used in both. The unpolarized beam, however, has higher energy and smaller energy spread than the polarized beam. To rectify this, a carbon wedge was placed in the beam at Position A of Fig. 1. Bragg-curve measurements gave the polarized beam energy as 165 ± 3.1 Mev (Group III')* and the unpolarized as 165 ± 2.8 Mev (Group III).* A copper (rather than carbon) first target was used in the hope that the smaller diffraction pattern would result in larger $\langle T_{20} \rangle$ at the first-scattering angle.

The distance from the target to counter No. 1 was always about 38 inches.

The accidental coincidence rate was in all cases very small.

H. Discussion of Uncertainties

The absolute values of I_0 are uncertain to about 10%. This uncertainty is chiefly due to the uncertainties in the extrapolation of the counting rate to zero absorber and in the slope of the voltage plateaus.

Because of the preponderance of inelastic scattering at large angles, the tabulated values of I_0 must there be interpreted as, at best, upper limits to the true values of the elastic cross section. The errors quoted are derived from counting statistics alone. The asymmetries observed with the unpolarized beam in the α experiment can be used to make an estimate of the systematic error in e in the following way. Let us assume that the asymmetries calculated from the unpolarized data are due to small misalignment errors. If we define

$$\beta(\Theta) = \frac{d}{d\Theta} \ln I_0(\Theta),$$

then to first order, and for $e^2 << 1$, the error Δe produced in the asymmetry by an angular misalignment ϵ is given by $\Delta e = \beta\epsilon$. From the unpolarized data, we compute $\epsilon_{rms} \simeq 0.135^{\circ}$. Using this value

---

* The Group designations are explained in Section II-1 and Table VI.

of ϵ_{rms}, we obtain values of $(\Delta e)_{rms} = \beta\epsilon_{rms}$ for our data. These are listed in Table I.

One may also compute values of B for the unpolarized beam. These are listed in Table II. Four of the eight are greater than their statistical uncertainties, the worst being about 1.7 times its uncertainty. Thus we are inclined to believe that, in the experiments with the polarized beam, we have observed no values of B inconsistent with zero.

The α experiment depends critically on matching the beam energies and energy spreads of the polarized and unpolarized deuteron beams. Although the counting rate due to elastic scattering should be independent of small variations of beam energy, that due to inelastic scattering is not. Crude estimates of the inelastic contamination based on a range curve taken at $\Theta = 17^{\circ}$ indicate that a disparity in beam energies of 1 Mev can give rise to an error of 0.02 in α. It is reasonable to suppose that drift in the steering-magnet field and main cyclotron field could give rise to a change in beam energy of at least 0.5 Mev. Thus, the observed values of α (Table IV) are consistent with $\alpha = 0$.

Table I

Estimate of rms systematic error in asymmetry. E is the beam energy.

E (Mev)	Tgt. No. 2	Θ	$(\Delta e)_{rms}$	E (Mev)	Tgt. No. 2	Θ	$(\Delta e)_{rms}$
165	C	9	0.084	133	Be	14	0.021
		10	0.069			18	0.027
		11	0.065			22	0.030
		14	0.041			26	0.016
		17	0.029	100	C	4	0.104
		18	0.029			7	0.061
		20	0.025			10	0.030
		24	0.025			14	0.067
		28	0.025			18	0.010
	Al	8	0.072			22	0.009
		12	0.032			26	0.025
		16	0.021			30	0.022
		18	0.035			34	0.019
		20	0.042		Al	4	0.207
		24	0.023			7	0.076
		28	0.023			10	0.062
		32	0.023			14	0.023
	Cu	17	0.026			18	0.000
		21	0.034			22	0.031
		25	0.027			26	0.014
133	C	4	0.056			30	0.015
		7	0.049			34	0.021
		10	0.049				
		14	0.040				
		18	0.011				
		22	0.025				
		26	0.025				
		30	0.025				

Table II

Values of B observed with unpolarized beam.

Target	Θ (degrees)	$\lvert B \rvert$
C	9	0.0013 ± 0.0085
	11	0.0049 ± 0.0088
	17	0.0088 ± 0.0095
	17	0.0135 ± 0.0087
Cu	17	0.0114 ± 0.0078
	17	0.0086 ± 0.0082
	21	0.0065 ± 0.0110
	25	0.0197 ± 0.0117

I. Discussion of Results

The results appear in Tables III and IV and in Figs.6 through 12. Beam polarizations are given in Table V. The data are divided into groups. Each time a critical parameter (snout collimator diameter, beam energy, etc.) was changed, a new group designation was assigned. Table VI gives the parameters characterizing each group as well as target thickness, rms angular resolution, and mean scattering energy for each of the experiments within the group.

Let us now compare our results with the predictions of the impulse approximation. We will make use of the unpolarized differential cross sections from Harvard[29] for the scattering of protons from carbon and aluminum at about 90 Mev and of the low-energy polarization data from Harwell,[33] for carbon and aluminum.

The following expressions relate the nucleon-nucleus scattering matrix to the quantities measurable at this energy:

$$I_0^n = |g_n|^2 + |h_n|^2 ,$$

$$I_0^n P = g_n^* h_n + g_n h_n^* ,$$

where I_0^n is the nucleon unpolarized scattering cross section, and P is the polarization.* It is seen, by comparing the above with the expression for I_0^d (Sect. II-A-2) that g and h enter into the expressions for I_0^d and I_0^n in different ways. We cannot predict I_0^d from I_0^n without a simplifying assumption. In view of the smallness of P at these energies, it is reasonable to assume that $|h|^2 << |g|^2$.

---

* It might be well at this point to underline the similarity between $i\langle T_{11}\rangle$ and P. Both are expectation values of spin operators. They point along the normal to the first scattering plane. The same sort of mechanism gives rise to both, and both are proportional to $I_0^{-1} (g^* h + g h^*)$.

Table III

Cross sections, asymmetries, polarizations for deuterons elastically scattered from lithium, beryllium, carbon, aluminum, and copper. Θ is second-scattering angle (lab); I_0 is unpolarized differential cross section (lab) (errors quoted are due to counting statistics only, and the absolute cross section is good to about 10%); e is asymmetry (quoted errors due to counting statistics only); B is as defined in Section I-D (errors due to counting statistics only); $i\langle T_{11}\rangle$ is vector-type polarization (errors include beam polarization statistics); group designation correlates data with those of Table VI.

Θ (degrees)	I_0 (mb/sterad)	e	B	$i\langle T_{11}\rangle$	Tgt 1	Grp.
Carbon at ~156 Mev						
9	1557 ± 13	-.010 ± .012	+.016 ± .008	-.017 ± .020	Cu	III'
10	877 ± 7	.017 ± .011	-.004 ± .012	.027 ± .017	Al	I
11	575 ± 3	.041 ± .008	+.007 ± .006	.062 ± .013	C	I
11	575 ± 8	.078 ± .014	-.008 ± .090	.117 ± .022	C	II
14	163 ± 3	.155 ± .021	+.042 ± .016	.242 ± .034	Al	I
17	94.2 ± 2.1	.319 ± .022	+.001 ± .020	.480 ± .046	C	II
17	103.6 ± 1.0	.253 ± .011		.480 ± .055	C	IV
18	82.0 ± 1.3	.283 ± .028		.426 ± .052	C	I
18		.287 ± .019	+.019 ± .035	.448 ± .035	Al	I
20	54.7 ± 0.5	.332 ± .019	-.004 ± .014	.499 ± .044	C	I
24	25.9 ± 0.7	.317 ± .035		.495 ± .058	Al	I
28	12.5 ± 0.4	.279 ± .028		.528 ± .078	C	IV
Aluminum at ~ 157 Mev						
8	2545 ± 24	-.033 ± .021		-.049 ± .031	C	I
12	400 ± 5	.225 ± .012	-.019 ± .012	.339 ± .029	C	I
16	242 ± 1	.233 ± .012	-.004 ± .011	.351 ± .030	C	I
16		.205 ± .016		.320 ± .013	Al	I
18	160 ± 2	.226 ± .009		.353 ± .020	Al	I
20	84.6 ± 1.4	.281 ± .030	+.008 ± .008	.422 ± .053	C	I
20		.278 ± .031		.434 ± .051	Al	I
24	36.6 ± 0.8	.450 ± .048		.677 ± .085	C	I
28	19.5 ± 1.0	.454 ± .069		.682 ± .134	C	I
32	9.30 ± 0.37	.378 ± .049		.567 ± .083	C	I

Table III continued

Θ (degrees)	I_0 (mb/sterad)	e	B	$i\langle T_{11}\rangle$	Tgt [1]	Grp.
Copper at ~157 Mev						
17	201 ± 8	.238 ± .038	+.016 ± .027	.357 ± .062	C	II
17	222 ± 2	.231 ± .041	+.002 ± .025	.389 ± .097	Cu	III'
21	111 ± 6	.299 ± .053	+.052 ± .037	.450 ± .086	C	II
21	105 ± 4	.335 ± .040	+.006 ± .026	.503 ± .069	C	II
21	121 ± 1	.272 ± .053	+.061 ± .038	.457 ± .119	Cu	III'
25	40.1 ± 2.3	.384 ± .059	+.011 ± .042	.577 ± .097	C	II
Lithium at ~121 Mev						
22	44.5 ± 1.1	.217 ± .025		.410 ± .064	C	VI
Beryllium at ~124 Mev						
14	302 ± 5	.045 ± .017		.084 ± .033	C	VI
18	105 ± 2	.164 ± .021		.310 ± .052	C	VI
22	55.5 ± 1.3	.273 ± .024		.517 ± .071	C	VI
26	29.7 ± 1.1	.255 ± .037		.483 ± .087	C	VI
Carbon at ~125 Mev						
4	12500 ± 200	-.016 ± .018		-.031 ± .035	C	VI
7	3860 ± 20	+.033 ± .019		+.063 ± .037	C	VI
10	1400 ± 20	.023 ± .014		.044 ± .027	C	VI
14	275 ± 7	.108 ± .024		.205 ± .050	C	VI
18	130 ± 4	.280 ± .032		.530 ± .083	C	VI
18	130 ± 3	.222 ± .020		.420 ± .059	C	VI'
22	77.0 ± 1.9	.256 ± .027		.484 ± .073	C	VI
26	37.6 ± 1.1	.323 ± .031		.612 ± .087	C	VI'
30	17.9 ± 0.8	.333 ± .042		.631 ± .104	C	VII'
Carbon at ~94 Mev						
4	27,900 ± 600	-.037 ± .019		-.070 ± .037	C	V
7	4,350 ± 40	-.055 ± .009		-.104 ± .020	C	V
10	1,770 ± 20	-.071 ± .009		-.135 ± .023	C	V
14	452 ± 8	-.032 ± .019		-.060 ± .036	C	V
14	438 ± 8	-.069 ± .019		-.130 ± .038	C	V
18	169 ± 4	+.095 ± .023		+.180 ± .048	C	V
22	152 ± 3	+.099 ± .022		+.188 ± .046	C	V
26	91.5 ± 2.5	.131 ± .028		.249 ± .059	C	V
30	47.0 ± 1.3	.164 ± .028		.311 ± .062	C	V
34	24.4 ± 1.3	.253 ± .051		.480 ± .110	C	V

Table III continued

Θ (degrees)	I_0 (mb/sterad)	e	$i\langle T_{11}\rangle$	Tgt	Grp.
Aluminum at ~94 Mev					
4	118,000 ± 1,000	+.020 ± .010	+.038 ± .019	C	V
7	6,650 ± 70	-.082 ± .011	-.155 ± .026	C	V
10	1,510 ± 20	-.097 ± .016	-.184 ± .036	C	V
14	388 ± 9	+.012 ± .023	+.022 ± .044	C	V
18	366 ± 9	-.039 ± .024	-.074 ± .045	C	V
22	212 ± 5	-.020 ± .020	-.038 ± .042	C	V
26	97.4 ± 2.9	+.105 ± .029	+.199 ± .059	C	V
30	73.1 ± 3.3	+.212 ± .046	+.401 ± .096	C	V
34	42.7 ± 2.5	+.170 ± .060	+.322 ± .118	C	V

Table IV

Values of α (see Section II-G). The first scattering was from a copper target. $\bar{E}$ is the mean scattering energy; α_{123} is derived from the 1-2-3 coincidence rate, α_{12} from the 1-2 rate. Errors quoted are due to counting statistics only. The unpolarized beam was Group III and the polarized beam was Group III'.

Target 2	Θ	α_{123}	α_{12}	$\bar{E}$ (Mev)
C	9°		$+.005 \pm .010$	159
Cu	17°	$+.026 \pm .027$	$+.040 \pm .023$	157
Cu	21°	$-.016 \pm .038$	$-.040 \pm .034$	157

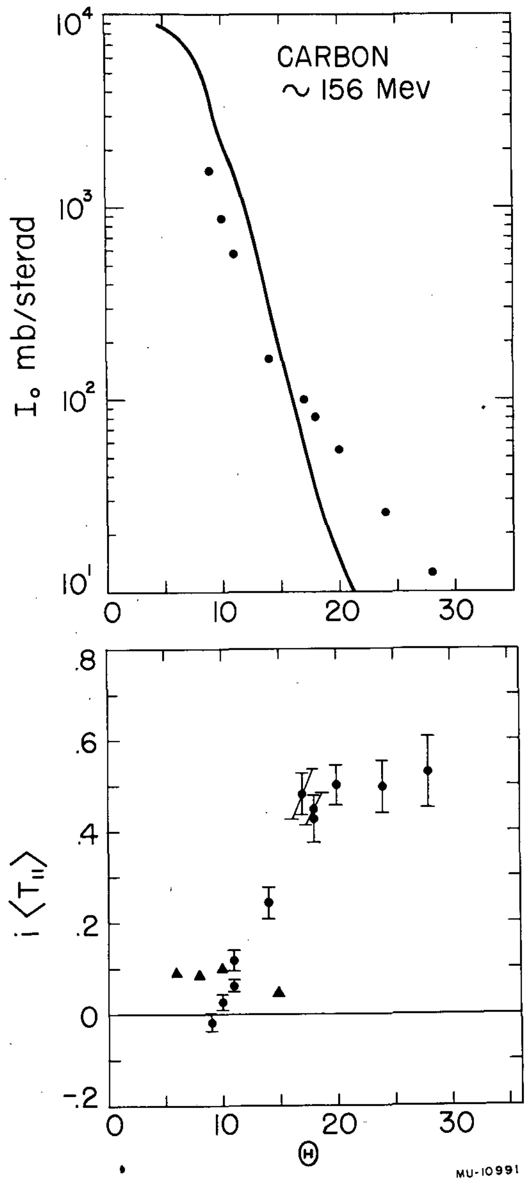

Fig. 6. Scattering of 156-Mev deuterons from carbon. Upper curve: cross section; lower curve: vector polarization. Triangular points and solid curve are predictions from proton data.

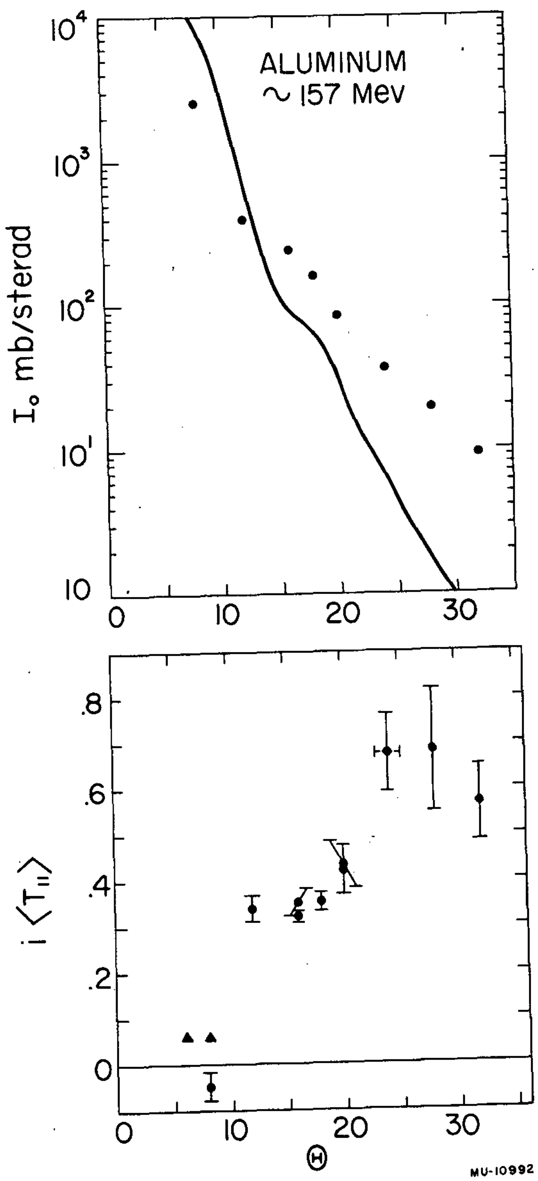

Fig. 7. Scattering of 157-Mev deuterons from aluminum. Upper curve: cross section; lower curve: vector polarization. Triangular points and solid curve are predictions from proton data.

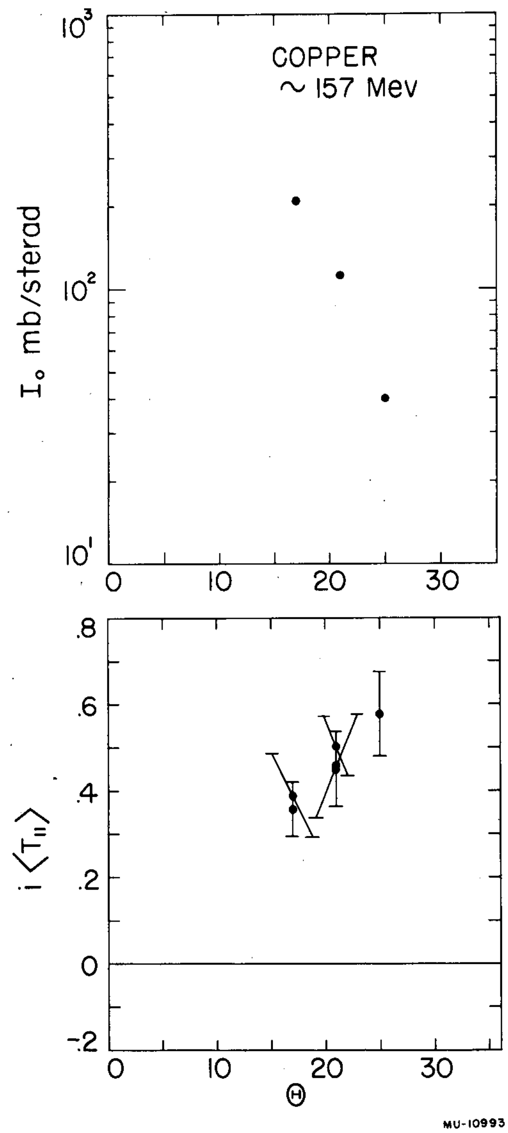

Fig. 8. Scattering of 157-Mev deuterons from copper. Upper curve: cross section; lower curve: vector polarization.

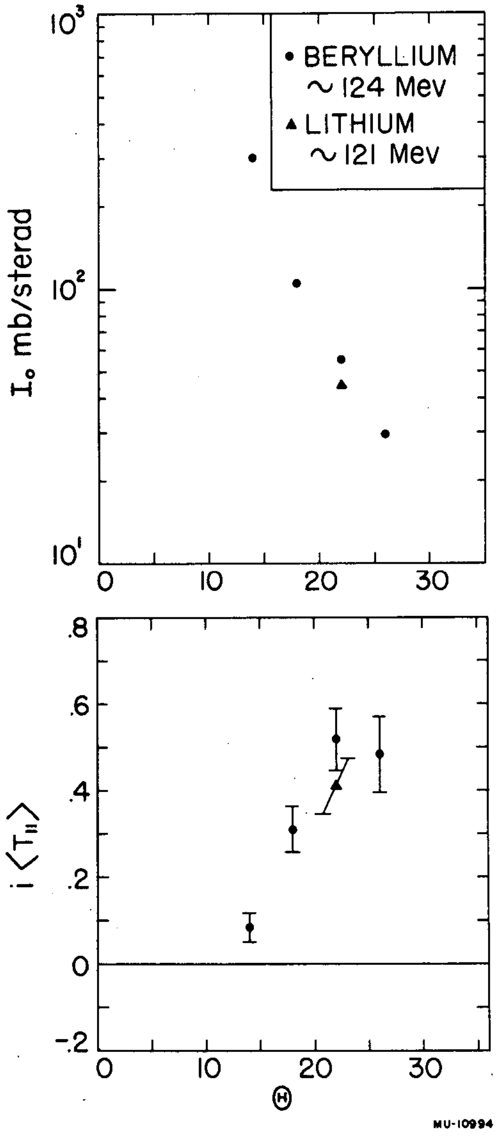

Fig. 9. Scattering of 124-Mev deuterons from beryllium. Upper curve: cross section; lower curve: vector polarization.

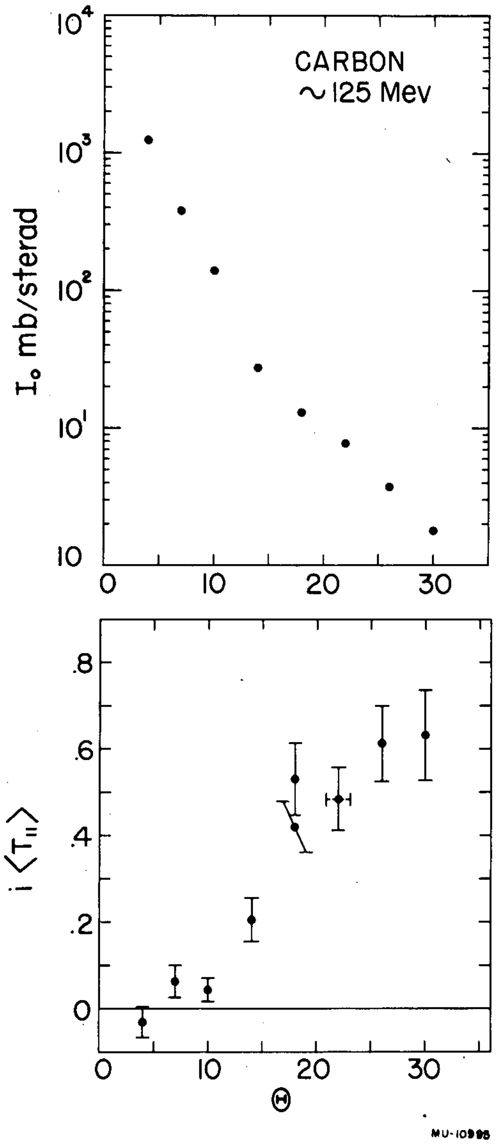

Fig. 10. Scattering of 125-Mev deuterons from carbon. Upper curve: cross section; lower curve: vector polarization.

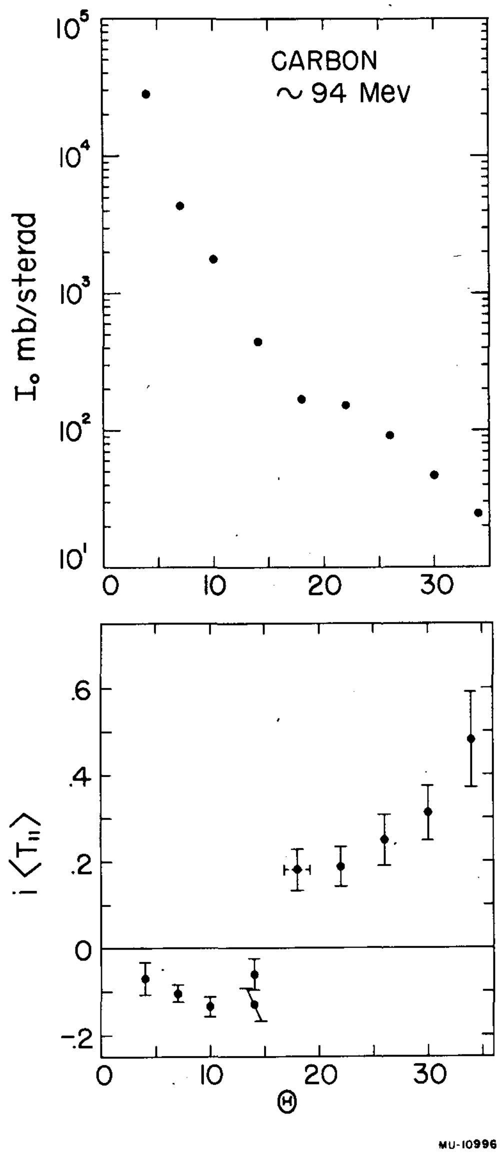

Fig. 11. Scattering of 94-Mev deuterons from carbon. Upper curve: cross section; lower curve: vector polarization.

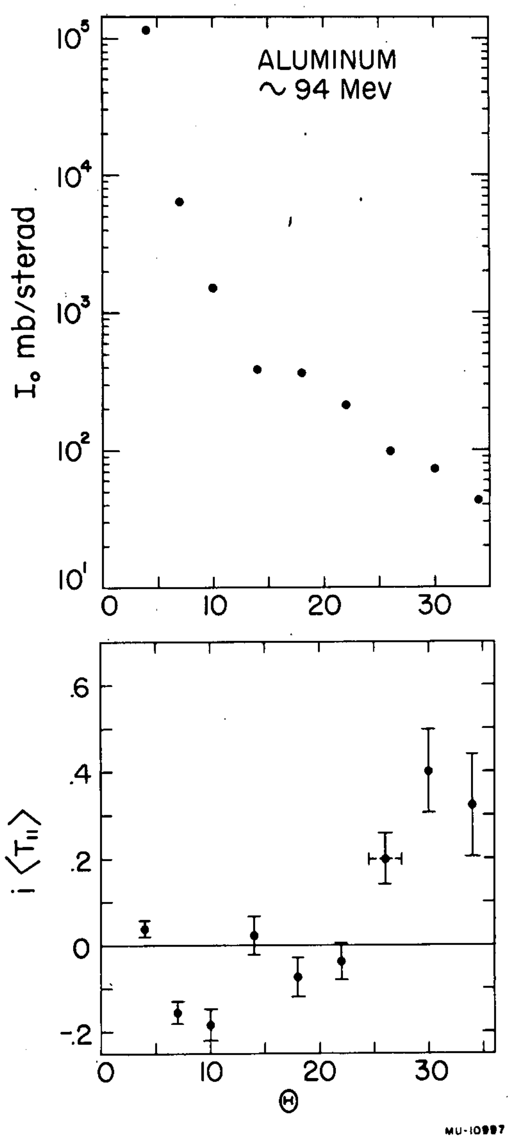

Fig. 12. Scattering of 94-Mev deuterons from aluminum. Upper curve: cross section; lower curve: vector polarization.

Table V

Beam polarizations. D is the diameter of the snout collimator. Errors are due to counting statistics only.

Tgt 1	D (in)	$i\langle T_{11}\rangle_1$	Groups
C	1	.333 ± .022	I - III'
Al		.320 ± .013	
Cu		.298 ± .052	
C	2	.264 ± .028	IV - VI'

Table VI

Parameters of the scattering. E is the beam energy and is followed by beam intensity; D is diameter of snout collimator; t is thickness of the second target; $\overline{E}$ is mean scattering energy; $\Delta\Theta$ is rms angular resolution.

Grp.	E (Mev)	Intensity (deuterons per second)	D (in.)	Tgt 1	Tgt 2	t (g/cm^2)	$\overline{E}$ (Mev)	$\Delta\Theta$ (degrees)
I	165 ± 2.6	8×10^4	1	C and Al	C	2.25	156	0.91
					Al	2.57	156	1.13
II	165 ± 3.4	8×10^4	1	C	C	1.59	159	0.83
					Cu	2.83	157	1.46
III	165 ± 2.8	---	1	---	C	1.59	159	0.83
					Cu	2.83	157	1.46
III'	165 ± 3.1	4×10^4	1	Cu	C	1.59	159	0.83
					Cu	2.83	157	1.46
IV	160 ± 5.5	5×10^5	2	C	C	2.25	151	1.20
V	100 ± 5.9	8×10^4	2	C	C	1.00	94	1.21
					Al	1.29	94	1.45
VI	133 ± 4.5	5×10^4	2	C	Li	2.83	121	1.22
					Be	2.12	124	1.18
					C	1.00	128	1.11
VI'	133 ± 4.5	5×10^4	2	C	C	2.00	124	1.26

On this basis we have

$$I_0^d (K) = 4 f (K)\left(\frac{M_d}{M_n}\right)^2 I_0^n (K) .$$

This appears as the solid curve in Figs. 6 and 7 (upper). When this expression for I_0^d is used, $i \langle T_{11} \rangle$ is given by

$$i \langle T_{11} \rangle = \frac{2}{\sqrt{3}} \frac{1}{4} \left(\frac{k_d}{k_n}\right)^2 \frac{\sin \theta_d}{\sin \theta_n} P .$$

The results of this calculation appear as the triangular points in Figs. 6 and 7 (lower).

The agreement is quantitatively poor. The theory predicts that $i \langle T_{11} \rangle \approx (3)^{-1/2}$ times the polarization for nucleons at half the deuteron energy. Proton polarizations are notoriously small below 95 Mev. At large angles $i \langle T_{11} \rangle$ becomes respectably large. The values of $i \langle T_{11} \rangle$ at 24° and 28° from aluminum at 157 Mev are near $(2)^{-1/2}$, which is the maximum value attainable if $\langle T_{21} \rangle = 0$.

Nor is there qualitative agreement. Since P should vary as $\sin \theta$ for small θ, the theory does not predict the observed change of sign of $i \langle T_{11} \rangle$ at small angles.* The observed and predicted values of I_0^d for carbon seem to run parallel to each other at small angles. At larger angles the observed values fall off much less rapidly than the predicted. The same sort of behavior is observed with aluminum.

It is interesting to plot $i \langle T_{11} \rangle$ in such a way as to facilitate the comparison of our results at different energies and different target nuclei. In Fig. 13 we have sketched a smooth curve through the experimental values for each element and energy, using as abscissa the value of the momentum transfer times the cube root of the target mass

---

* It is not likely that this rapid fall of $i \langle T_{11} \rangle$ as θ decreases is due to Coulomb scattering. The cross-section data from Harvard[29] indicate that Coulomb scattering becomes important at angles much smaller than any at which we have made measurements.

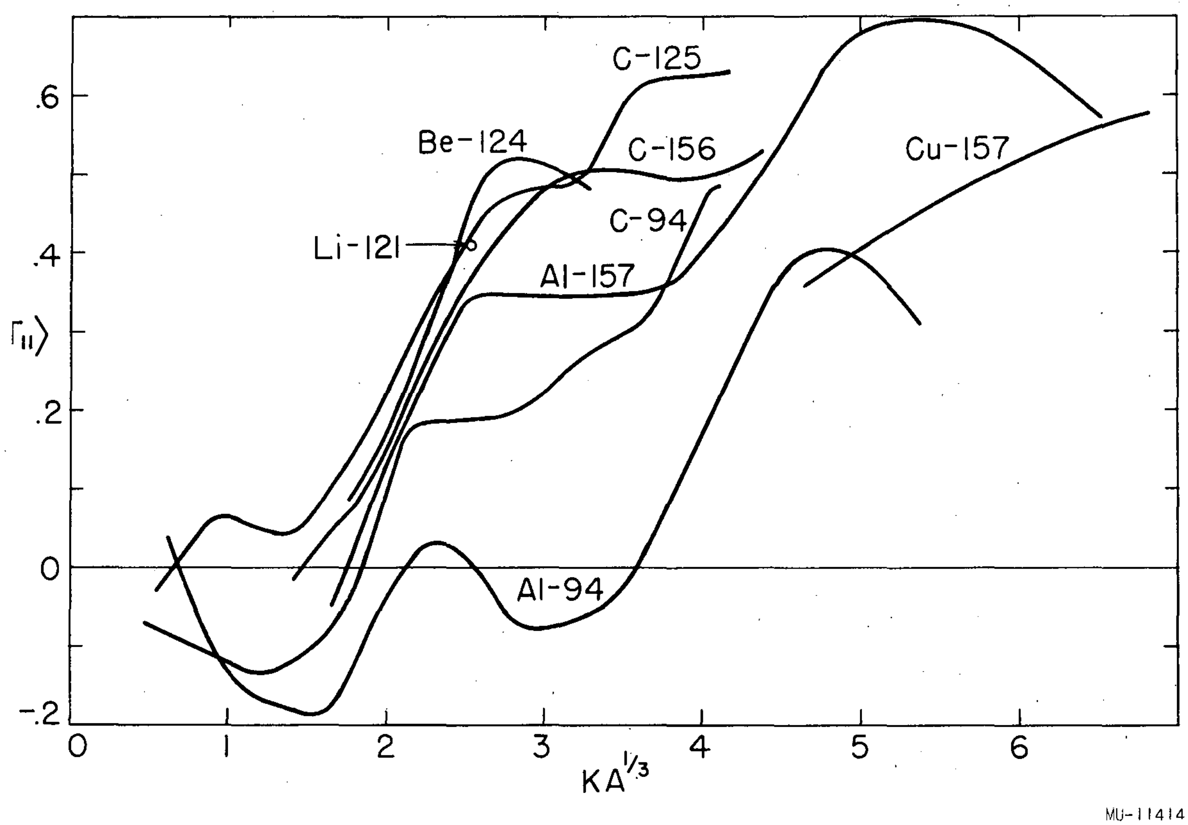

Fig. 13. Composite of all i $\langle T_{11}\rangle$ data, plotted against $KA^{1/3} = 2\,k \sin \frac{1}{2}\theta\, A^{1/3}$. The number following the element symbol is the mean scattering energy in Mev.

number. It is seen that there is a good deal of similarity between the curves. The rapid fall-off of $i\langle T_{11}\rangle$ with decreasing K is a quite consistent feature, and is centered in all cases around $K A^{1/3} = 2.$* The lowering of the energy from 156 to 94 Mev seems to result in a general depression of $i\langle T_{11}\rangle$.

The reason for the disparity between the theoretical and experimental results is not understood. It is unlikely that the trouble can be traced to multiple collisions of a single nucleon within the target nucleus, since we have used empirically derived nucleon amplitudes in our calculations. Dr. Malvin A. Ruderman has attempted to use the presence of D state in the deuteron wave function to explain the change of sign of the polarization at small angles, with very little success so far. It is possible that inclusion in the theory of the possibility for simultaneous scattering of both nucleons of the deuteron would lead to enhancement of the large-angle cross section and polarization. There is one other refinement of the impulse approximation, which is suggested by the following observations. An imaginary part is usually included in the nucleon-nucleus potential. This is used to describe the effect of inelastic events in which the target nucleus is left in an excited state. We would expect to find, in the equivalent deuteron — nucleus potential, an additional imaginary part describing inelastic events in which the deuteron was dissociated. The impulse approximation does not seem to predict this. The inclusion of the attenuation of the deuteron wave by this sort of stripping reaction as the wave traverses the target nucleus should also lead to enhancement of the large-angle polarization. Although the consideration of these two effects should operate to reduce the difference between theory and experiment, we do not know whether it results in quantitative agreement. Indeed, it is very unlikely that we can, by this means, explain the small-angle change of sign of the polarization.

---

*K is measured in units of 10^{13} cm^{-1}.

III. PROTON–PROTON DOUBLE SCATTERING

A. Apparatus

In this experiment, a snout collimator of rectangular cross section was used. This collimator had a vertical dimension of 2 inches and a horizontal of 0.5 inch, which enabled us to obtain a fairly intense beam ($\sim 1.5 \times 10^4$ protons/sec) and obtain good energy and angular resolution.

On the scattering table was mounted a vertical post on which was centered a calibrated azimuth sector. This post served as a pivot for the scattering arm. A movable railroad allowed one to move the liquid H_2 target, the blank target, a Be target, or no target at all to a position over the pivot. The change of ϕ by 180° was accomplished by swinging the counter arm to the opposite side of the beam, rather than by rotating it about the beam axis, as was done in the deuteron experiments. The counter arm position was read on the azimuth sector.

The liquid-hydrogen target used was that described by Garrison.[27] The target is a cylinder whose walls are of 4-mil stainless steel. It is 5.6 inches in diameter ($\simeq 1.0$ g/cm^2 of liquid H_2), and 8 inches in height. It is enclosed in a vacuum jacket of 1/8-inch dural. The beam enters and leaves the jacket through circular dural windows, 3 inches in diameter and 5 mils thick.

B. Alignment

The beam axis was determined by using two x-ray films, in a manner similar to that used in the deuteron experiments. The transit was then lined up on—and subsequently used to define—the beam. The scattering table was moved to place the pivot directly below the beam axis. With the target centered on the beam, the counting rate was measured for small angles, with Counters A and B used as monitor. It is seen from Fig. 2 that this sort of measurement is capable of determining the true zero of Θ to an accuracy of somewhat less than 0.1°.

C. Range Curve

In the polarization check (described in the next subsection), a Be second target was used. Here the range curve was taken in the beam, as in the deuteron experiments, and the same considerations apply. The absorber was corrected for recoil and target-thickness changes.

In scattering from H_2, however, the problem of inelastic scattering did not exist, and it was not necessary to take the range curve in the beam. The range curves were taken at the actual scattering angles used, and a new one was taken each time Θ was changed. In this case, the absorber was not necessary for separating elastic from inelastic scattering, but served simply to reduce the ratio of effect to background. Consequently, the choice of absorber was not as critical as in elastic scattering from complex nuclei, and one must only be careful not to bias out one side of the beam by operating too near the knee.

D. Procedures

With the beam degraded at position A, measurements of the p-p asymmetry were made at laboratory-system angles 10°, 15°, 22.5°, 30°, and 35°. Several separate runs were made at each angle.

It was felt that a daily check of the beam polarization would be desirable. To this end, a measurement of the asymmetry in the scattering at 13° from a 2.18 g/cm^2 Be target was made at the beginning of each running day. These checks were in good agreement with each other.

In order to determine whether the angle of the first scattering of the beam entering the cave differed from that of the full-energy beam, by virtue of the energy degradation suffered before entering the exit tube, a further check was made. The absorber at Position A was removed, and a graphite plug was fastened to the cyclotron end of the snout collimator (Position B of Fig. 1). With the beam degraded in this position, another measurement of the asymmetry in scattering from Be was made. The energies of the two beams were

Degraded at Position A: 174 ± 10 Mev,
Degraded at Position B: 185 ± 17 Mev.

The asymmetries observed were

Weighted average, Position A $e = 0.443 \pm .013$,
Weighted average, Position B $e = 0.437 \pm .014$.

The difference between the two is not statistically significant. The polarization of the 174-Mev beam was therefore taken to be the same as that of the full-energy beam.

The Blank/Target ratio varies from about 0.35 at $\Theta = 10^{\circ}$ to about 0.10 at $\Theta = 35^{\circ}$ for H_2 runs, and was about 0.05 for the Be runs. The accidental rate was negligible in all runs.

The distance from target to counter No. 1 was about 52 inches.

E. Beam Polarization

The results of this experiment have appeared in the Physical Review.[28] In that article we assumed a proton first-scattering angle of 13° and a beam polarization of 0.76. As already indicated, however, the angle is actually 10.25°. No identical double scattering from Be has been performed at this angle. Beryllium polarizations for $\Theta = 9^{\circ}$, 13°, 15°, 17°, and 19° are given by Tripp.[23] It was decided to interpolate between the 9° and 13° points with the shape-independent Born approximation of Fermi.[13] This approximation predicts a polarization of the form

$$P = \frac{2\alpha \epsilon \sin \theta}{1 + \epsilon^2 + \alpha^2 \sin^2 \theta},$$

where α and ϵ are constants independent of θ. These two constants allow one to fit the data at two points; 9° and 13° were used for this purpose. The experimental points fall off more rapidly beyond 13° than does the interpolation function. This is presumably due to the existence of a broad polarization minimum centered somewhere out past 19°. It is hoped that the presence of this minimum is not too strongly felt in the region under consideration. When the interpolated polarization is converted to an asymmetry by multiplication by 0.76 and the square root of the result extracted, one obtains the corrected beam polarization as $0.733 \pm .008$. The error is determined from the counting statistics of the 9° and 13° points, and is smaller than the error assigned to either of those points. This is a result characteristic of the interpolation process.

If we assign the following errors:

counting statistics	0.01.
poor choice of interpolation function	0.02,
uncertainty in scattering angle	0.01*,
inelastic contamination	0.02*,

we obtain a total uncertainty of 0.03. We therefore take the beam polarization to be $0.73 \pm .03$.

---

* Following Appendix I in the paper by Tripp.[23]

F. Angular Resolution

The four contributions to the angular resolution that were considered were:

1. Target size,
2. Beam size ,
3. Counter size,
4. Multiple scattering in the target.

The geometrical angular resolution of the proton-proton scattering was determined by folding together the projection of the illuminated target volume and the resolution of the defining counter. In the p-Be scattering, the contribution due to target size was ignored and the geometrical angular resolution computed by folding together two slits, one the width of the beam, the other the width of the defining counter. The multiple scattering was in both cases computed by using the thin-target approximation

$$\theta_{rms} = 0.95 \sqrt{(Z+1) \frac{\Delta E}{E}} ,$$

where θ_{rms} is the rms projected multiple scattering angle in degrees; Z the target atomic number, ΔE the energy loss in the target, and E the mean energy.

G. Discussion of Uncertainties

As previously noted, the error Δe produced in the asymmetry by an angular misalignment ϵ is given by the approximate relation

$$\Delta e = \frac{1}{I_0} \frac{dI_0}{d\Theta} \cdot \epsilon ,$$

where I_0 is the unpolarized cross section in the laboratory system. If we assume I_0 = constant in the c. m. system, then I_0 = constant x cos Θ in the laboratory system, and we have

$$(\Delta e)_{rms} = \tan \Theta \cdot \epsilon_{rms}$$

The sources of misalignment error considered are:

1. Magnetic field in the cave,
2. Failure of the axis of the counter-arm pivot to intersect the beam axis,
3. Uncertainty in the determination of the zero of Θ.

If the magnetic field in the cave were uniform, and if the protons lost no energy in the target, the existence of the magnetic field would have no effect on the asymmetry. Neither assumption is true. We shall assume that the former is true—that the magnetic field is uniform with a magnitude of 15 gauss. The maximum misalignment occurs at $\Theta = 35^o$, and is 0.35×10^{-3} radian. The positioning of the counter-arm pivot and determination of the beam center are believed good to within 1/16 inch. The maximum misalignment again occurs at $\Theta = 35^o$, and is $\epsilon = 0.22 \times 10^{-3}$ radian. The zero of Θ can be determined to within $0.1^o = 1.75 \times 10^{-3}$ radian. Thus

$$\epsilon_{rms} = \sqrt{\sum_i \epsilon_i^2} = 1.8 \times 10^{-3} \text{ radian.}$$

Taking the maximum value of Θ used, we obtain

$$(\Delta e)_{rms} = \tan 35^o \times 1.8 \times 10^{-3} = 1.3 \times 10^{-3}.$$

Thus, the systematic errors in e are about a factor of 10 lower than the counting statistics and can be neglected.

H. Discussion of Results

The results are listed in Table VII and displayed in Fig. 14. The errors quoted for e are those due to counting statistics only. The errors in P, however, include the beam polarization uncertainty (which includes systematic errors).

The energy lost by a beam of 174-Mev protons in passing through 1.0 g/cm^2 of hydrogen is 10.3 Mev. Thus, the mean scattering energy is 169 Mev.

If one stays out of the region where Coulomb effects are important, he may express the product of the proton-proton polarization and unpolarized cross section in the form

$$I_0 P = \sin\theta\cos\theta \sum_{n=0}^{\infty} b_{2n} \cos^{2n}\theta .$$

A least-squares fit was made to the data by assuming that I_0 was independent of θ in the region under consideration, having the value 4.16 mb/sterad,[5] and that only b_0 and b_2 were important. The weighting factors were computed from the counting statistics on the asymmetries only. The result of the calculation is

$$b_0 = 1.36 \pm 0.37 \text{ mb/sterad},$$
$$b_2 = 1.30 \pm 0.61 \text{ mb/sterad},$$

where the errors are rms values and reflect counting statistics in the asymmetries only. These numbers should perhaps not be taken too seriously, since inclusion of the third term considerably alters the above results. The result of this calculation is

$$b_0 = +1.98 \pm 0.64 \text{ mb/sterad},$$
$$b_2 = -1.97 \pm 2.88 \text{ mb/sterad},$$
$$b_4 = +3.31 \pm 2.85 \text{ mb/sterad}.$$

This result suggests that in the attempt to determine phase shifts the polarization data had best be inserted as discrete points rather than Fourier coefficients. In Fig. 15 is plotted $e/\sin\theta\cos\theta$ vs $\cos^2\theta$.

Table VII

Polarization in proton-proton scattering at 169 Mev

Θ (degrees)	θ (degrees)	$\Delta\theta$ (degrees)	e	Δe	P	ΔP
10	20.8	1.9	0.183	0.025	0.251	0.036
15	31.3	2.5	0.169	0.015	0.232	0.023
22.5	46.8	3.4	0.162	0.022	0.222	0.032
30	62.2	3.9	0.137	0.024	0.188	0.034
35	72.4	4.7	0.071	0.028	0.097	0.038

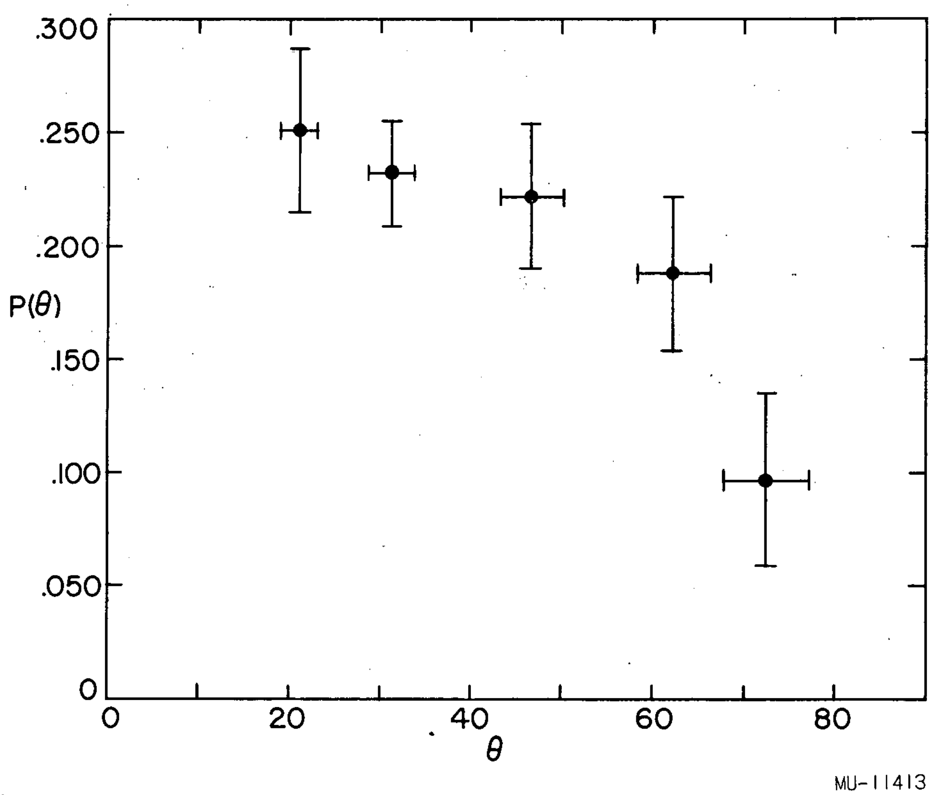

Fig. 14. Proton-proton polarization at 169 Mev vs center-of-mass angle θ.

At any rate, it is clear that there exist significant b_n with $n > 0$, which indicates considerable contribution to the scattering by waves of $L \geqslant 3$.

That this experiment, together with the experiments of Garrison[4,27] and Pettengill,[5] cannot be made to yield a unique set of phase shifts at 170 Mev may be seen from the following argument. The present experiment shows that a phase-shift analysis must include f waves. Thus, unless one is willing to assume values for some phase shifts, he must deal with nine of them. The number of independent pieces of information in the differential cross section is $L + 1 = 4$ (L being the maximum orbital angular momentum contributing to the scattering—in this case taken to be 3). From the polarization data there are obtainable three pieces of information. The total, seven, is insufficient to determine the nine phase shifts. (It is true that the work of Garrison contains information about the Coulomb-nuclear interference,[21] which is another piece of information, though somewhat difficult to make use of). It appears then, that any determination of the 170-Mev phase shifts must depend on either further experiments or plausible assumptions.

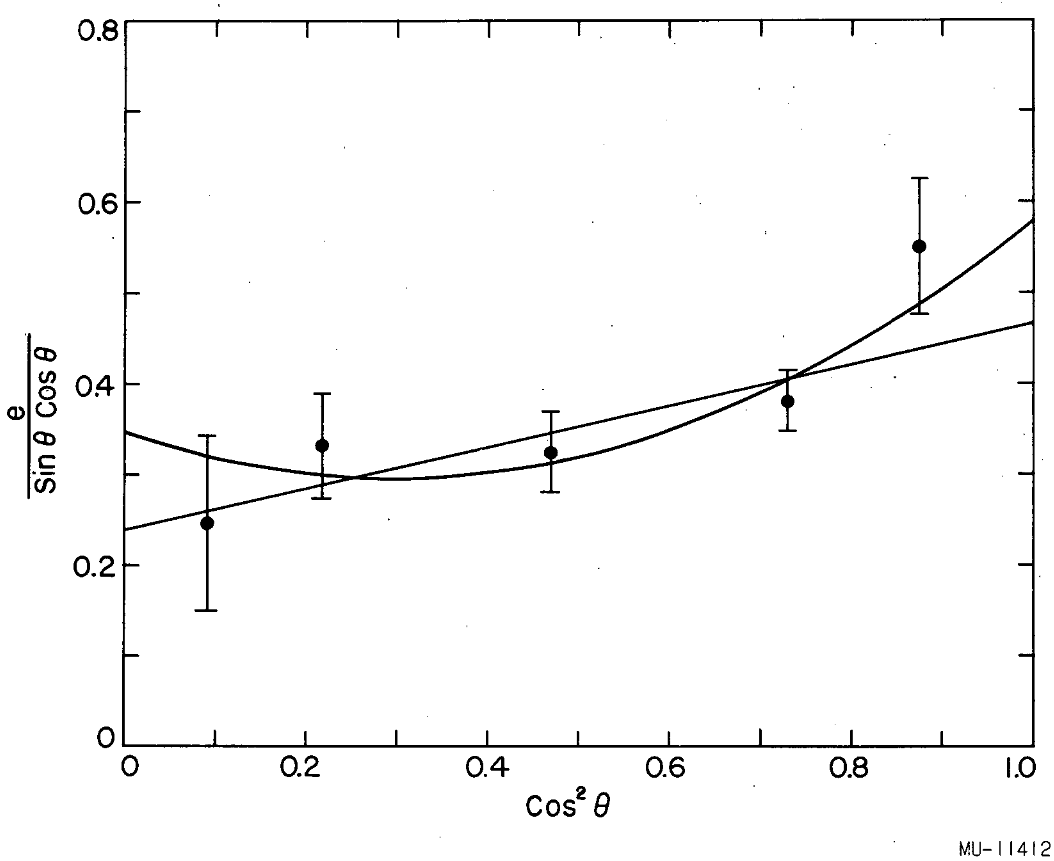

Fig. 15. e $(\theta)/\sin\theta\cos\theta$ vs $\cos^2\theta$. The solid straight and curved lines are the two- and three-parameter least-squares fits respectively.

ACKNOWLEDGMENTS

To Dr. Owen Chamberlain particular thanks are due for his advice and assistance throughout the experiments. The help of Dr. Clyde Wiegand—particularly with the electronics—has been invaluable. Dr. Emilio Segrè has contributed generously of his advice. The deuteron experiments were done in collaboration with Drs. Robert Tripp and Tom Ypsilantis, the proton experiment with Mr. David Fischer. Much assistance was provided by Mr. James Simmons.

Discussions with Dr. Lincoln Wolfenstein have been of great value in aiding my understanding of polarization theory.

The author is indebted to Dr. Karl Strauch for communicating the Harvard cross-section results before publication, and also to Dr. B. Rose for communicating to us results of the Harwell low-energy polarization experiments before publication.

Thanks are also due to the crew of the 184-inch cyclotron under Mr. James Vale for providing the polarized beam.

This work was done under the auspices of the United States Atomic Energy Commission.

APPENDIX

Effect of a Magnetic Field on the Deuteron Spin State

We wish here to investigate the effects of the fringing field of the cyclotron and the field of the bending magnet on the polarization state of the deuteron beam.

If a polarized beam of protons is subjected to a magnetic field parallel to the normal of the first-scattering plane, the polarization state of the beam is unaffected. Thus, in an experiment with polarized protons, one does not have to pay any attention to the deflection suffered by the first-scattered beam in the various magnetic fields. This is not the case with deuterons.

If we write the spin part of the wave function for a deuteron in a magnetic field along the y direction (in the representation in which S_z is diagonal) as

$$\Psi = \begin{pmatrix} \psi_1 \\ \psi_2 \\ \psi_3 \end{pmatrix},$$

then

$$\psi_1 = -\frac{i}{\sqrt{2}} \left(a\, e^{i\omega t} - b\, e^{-i\omega t} - c\right),$$

$$\psi_2 = a\, e^{i\omega t} + b\, e^{-i\omega t},$$

$$\psi_3 = +\frac{i}{\sqrt{2}} \left(a\, e^{i\omega t} - b\, e^{-i\omega t} + c\right)$$

is the most general such wave function. We fix the phase of Ψ by choosing $c = c^*$. If we demand that at time $t = 0$ (the time of the first scattering) $\langle S_x \rangle = \langle S_z \rangle = 0$, then either $a^* = b$ in which case $\langle S_y \rangle = 0$, or $c = 0$. In the former case,

$$\left.\begin{aligned} \langle S_x \rangle &= 0 \\ \langle S_y \rangle &= 0 \\ \langle S_z \rangle &= 0 \end{aligned}\right\} \quad \text{for all } t,$$

and in the latter,

$$\left.\begin{aligned}\langle S_x\rangle &= 0\\ \langle S_y\rangle &= 2\ (\ |a|^2 - |b|^2)\\ \langle S_z\rangle &= 0\end{aligned}\right\}\ \text{for all } t.$$

Thus, in reactions such as we are considering, in which the first-scattered deuterons are subjected to a magnetic field parallel to the normal to the first-scattering plane, the components of $\langle\vec{S}\rangle$ are unaffected by the field.

There is, however, an effect on the tensor components of polarization — the $\langle T_{2M}\rangle$. Here, two factors must be considered.

1. The $\langle T_{2M}\rangle_1$ that result from the first scattering are referred to a set of coordinates having z axis along $\vec{k}_{1f}$, whereas we must refer them to coordinates having z axis along $\vec{k}_{2i}$ —the direction in which the beam actually enters the cave.

2. The effect of the magnetic field on the spins themselves is to rotate the principal axes of the tensor $\langle S_i S_j\rangle$.

These two effects produce the same result on the $\langle T_{2M}\rangle$, but in opposite directions and with different magnitudes.

If the $\langle T_{2M}\rangle$ resulting from the first scattering and referred to a z axis along $\vec{k}_{1f}$ are designated $\langle T_{2M}\rangle_1$, and the $\langle T_{2M}\rangle$ entering the cave and referred to a z axis along $\vec{k}_{2i}$ are designated $\langle T_{2M}\rangle_1'$, then

$$\langle T_{22}\rangle_1' = 1/2\,(1+\cos^2\lambda)\langle T_{22}\rangle_1 - 1/2\sin 2\lambda\langle T_{21}\rangle_1 + 1/2\sqrt{3/2}\,\sin^2\lambda\,\langle T_{20}\rangle_1\ ,$$

$$\langle T_{21}\rangle_1' = 1/2\sin 2\lambda\langle T_{22}\rangle_1 + \cos 2\lambda\langle T_{21}\rangle_1 - 1/2\sqrt{3/2}\,\sin 2\lambda\langle T_{20}\rangle_1\ ,$$

$$\langle T_{20}\rangle_1' = \sqrt{3/2}\,\sin^2\lambda\,\langle T_{22}\rangle_1 + \sqrt{3/2}\,\sin 2\lambda\langle T_{21}\rangle_1 + (1-3/2\sin^2\lambda)\,\langle T_{20}\rangle_1\ ,$$

where $\lambda = (\mu - 1)\,\eta$,

$\mu = +\,0.85647$ = deuteron magnetic moment, in nuclear magnetons,

η = the total angular deflection of the beam, considered positive when directed opposite to the normal to the first-scattering plane, $\vec{n}_1$.

In this experiment $\eta = 39.5^{\circ}$ and $\lambda = -\,5.67^{\circ}$.

BIBLIOGRAPHY

1. Chamberlain, Segrè, Tripp, Wiegand, and Ypsilantis, Phys. Rev. 93, 1430 (1954).
2. Chamberlain, Segrè, Tripp, Wiegand, and Ypsilantis, Phys. Rev. 98, 840 (1955).
3. H. P. Stapp, The Theory and Interpretation of Polarization Phenomena in Nuclear Scattering (Thesis), UCRL-3098, Aug. 1955.
4. Chamberlain and Garrison, Phys. Rev. 95, 1349 (1954).
5. G. Pettengill, Measurements on Proton-Proton Scattering in the Energy Region 150 to 340 Mev (Thesis), UCRL-2808, Dec. 1954.
6. Dickson and Salter, Nature 173, 946 (1954).
7. J. Baskir, Proceedings of Fifth Annual Rochester Conference, Interscience, Dec. 1954.
8. Marshall, Marshall, and de Carvalho, Phys. Rev. 93, 1431 (1954).
9. Kane, Stallwood, Sutton, Fields, and Fox, Phys. Rev. 95, 1694 (1954).
10. Chamberlain, Donaldson, Segrè, Tripp, Wiegand, and Ypsilantis, Phys. Rev. 95, 850 (1954).
11. Oxley, Cartwright, and Rouvina, Phys. Rev. 93, 806 (1954).
12. Wolfenstein and Ashkin, Phys. Rev. 85, 947 (1952).
13. E. Fermi, Nuovo Cimento 11, 407 (1954).
14. R. M. Sternheimer, Phys. Rev. 100, 886 (1955).
15. Chamberlain, Segrè, Tripp, Wiegand, and Ypsilantis, Phys. Rev. 95, 1104 (1954).
16. W. Lakin, Phys. Rev. 98, 139 (1955).
17. L. Schiff, Quantum Mechanics, McGraw - Hill, 1949, Sect. 18.
18. Dalitz, Proc. Physical Soc. of London A65, 175 (1952).
19. G. F. Chew, Phys. Rev. 80, 196 (1950).
    G. F. Chew and G. C. Wick, Phys. Rev. 85, 636 (1952).
20. G. F. Chew, Phys. Rev. 74, 809 (1948).
21. A. Garren, Phase Shifts and Coulomb Interference Effects for High-Energy Proton-Proton Scattering, Carnegie Institute of Technology, Report No. NYO-7102, March 1955.

22. T. J. Ypsilantis, Experiments on Polarization in Nucleon-Nucleon Scattering at 310 Mev (Thesis), UCRL-3047, June 1955.

23. R. D. Tripp, Elastic Scattering of High-Energy Polarized Protons by Complex Nuclei (Thesis), UCRL-2975, April 1955.

24. L. Wolfenstein, Phys. Rev. 75, 1664 (1949).

25. L. Wolfenstein, Phys. Rev. 96, 1654 (1954).

26. Blatt and Weisskopf, Theoretical Nuclear Physics, New York, 1952, Chapt. VIII.

27. J. D. Garrison, Proton-Proton Scattering Experiments at 170 and 260 Mev (Thesis), UCRL-2659, July 1954.

28. Fischer and Baldwin, Phys. Rev. 100, 1445 (1955).

29. K. Strauch and F. Titus, private communication; Gerstein, Niederer, and Strauch, private communication.

30. Millburn and Schecter, Graphs of RMS Multiple Scattering Angle and Range Straggling for High-Energy Charged Particles, UCRL-2234, Jan. 1954.

31. Chamberlain, Segrè, and Wiegand, Phys. Rev. 83, 923 (1951).

32. K. A. Brueckner, Phys. Rev. 89, 834 (1953).

33. Dickson, Rose, and Salter, Proc. Phys. Soc. 68A, 361 (1955); and private communication.